

Spatio-temporal performance evaluation of 14 global precipitation estimation products across river basins in southwest Iran

Akbar Rahmati¹, Aydin Bakhtar², Afshin Shayeghi³, Zahra Kalantari^{4&5*}, Alireza Massah Bavani¹, Navid Ghajarnia⁵

¹ Department of Irrigation and Drainage Engineering, College of Abureyhan, University of Tehran, Iran

² Department of Water Engineering, Urmia University, Urmia, Iran

³ Water Engineering Department, Imam Khomeini International University (IKIU), Qazvin, Iran

⁴ Department of Sustainable Development, Environmental Science and Engineering (SEED), KTH Royal Institute of Technology, Stockholm, Sweden

⁵ Department of Physical Geography, Bolin Centre for Climate Research, Stockholm University, SE-10691, Stockholm, Sweden

*Corresponding author: Zahra Kalantari (zahrak@kth.se)

Abstract

Access to spatio-temporally consistent precipitation data is a key pre-requisite for hydrological studies, especially in data-scarce regions. Different global precipitation products offer an alternative way to estimate precipitation over areas with inadequate gauge distributions. However, before use of the datasets, the accuracy of these global estimations must be carefully studied at local and regional scale. This study evaluated 14 global precipitation products against gauge observations 2003-2012 in Karun and Karkheh basins in southwest Iran. Different categorical and statistical indices, including Kling-Gupta Efficiency (KGE), bias, correlation coefficient, and variability ratio, at varying spatial and temporal resolution were used to evaluate the products. KGE results at both daily and monthly time steps suggested that TMPA-3B42V7.0 and MERRA-2 outperformed all other products, while CMORPH-BLDV1.0 and PERSIANN-CDR was the best-performing product at daily and monthly time steps, respectively. ERA5-Land showed the highest positive bias compared with in-situ observations, particularly for mountainous southeastern parts of Karun basin. Overall, bias-adjusted products obtained by merging ground-based observations in the estimations outperformed the unadjusted versions. The spatial distribution of statistical error metrics indicated that almost all products showed their greatest uncertainties for mountainous regions, due to complex precipitation processes in these regions. These results can significantly contribute to various hydrological and water resources planning measures in the study region, including early flood warning systems, drought monitoring, and optimal dam operations.

Keywords: Global precipitation estimation products; Spatio-temporal performance evaluation; Statistical error analysis; Categorical index; Iran.

31 **Highlights**

- 32 • MERRA-2 is the most accurate product to represent daily precipitation across southwest of Iran
- 33 • TMPA-3B42V7.0 is the most accurate product at monthly time scale in Karun and Karkheh basins
- 34 • ERA5-Land showed highest bias versus observational data
- 35 • All products showed their greatest uncertainties across mountainous areas

1. Introduction

Surface runoff, soil moisture, evapotranspiration, groundwater recharge, and several other hydro-climatic variables are directly or indirectly influenced by precipitation amount and intensity (Ghajarnia et al., 2020; Kalantari et al., 2019). Owing to its close interactions with other land-atmospheric variables, reliable estimation of precipitation is of special interest and critical importance in a variety of fields, such as water resources management, hydrological modeling, global energy analysis, climate modeling, and agricultural studies (Asante et al., 2007; Carrera-Hernandez and Gaskin, 2007; Funk et al., 2014; Huffman et al., 1997; Kucera et al., 2013; Zhang et al., 2012). Ground-based observations provide the most accurate precipitation measurements (Sun et al., 2018). However, in inaccessible and remote areas and in many developing countries, estimates of gauge records are either incomplete or non-existent, mostly due to the high cost of gauge installation and maintenance (Salio et al., 2015; Sun et al., 2018). These spatial gaps in precipitation measurements, together with the common inconsistencies in gauge records, make it difficult to provide an unbiased view of precipitation at global scale (Brunetti et al., 2006).

Different high-resolution precipitation products have been developed in recent decades, with increasing use of remote sensing techniques and enhanced computational capacities. These state-of-the-art global and quasi-global precipitation estimation products can be classified into four categories: 1) reanalysis products (Hersbach et al., 2020; Kalnay et al., 1996; Kobayashi et al., 2015; Rienecker et al., 2011); 2) gridded ground-based observations (Harris et al., 2014; Huffman et al., 1997; Schneider et al., 2008; Yatagai et al., 2012); 3) satellite-based products (Hou et al., 2014; Huffman et al., 2007; Joyce et al., 2004; Sorooshian et al., 2000); and 4) Climate Data Records (CDRs) (Ashouri et al., 2015; Beck et al., 2019b). Although these spatio-temporally consistent products are potentially good alternatives for ground-based observations and can

address some of the disadvantages and uncertainties of gauge records, they must be examined thoroughly before use to ensure their reliability and accuracy (Shayeghi et al., 2020; Sun et al., 2018). It is reported that the performance of these products varies by region (Duan et al., 2016), since climate patterns differ from one region to another. Therefore, numerous studies have focused on evaluating the performance of these products across different regions of the world with varying geographical and climatic conditions. These studies have been carried out at different spatial extents, including global, regional, and local scale (Awange et al., 2019; Azizian and Ramezani Etedali, 2019; Beck et al., 2019a; Ghajarnia et al., 2015; Hosseini-Moghari et al., 2018; Satgé et al., 2020; Sun et al., 2018). In addition to evaluations, these studies have also made comparative analyses of different technologies and algorithms of precipitation estimates, and improvements in these over time.

Many previous studies have evaluated precipitation estimation products for some basins or the entire country of Iran. An early study by Javanmard et al. (2010) evaluated the performance of TMPA-3B42 precipitation estimations against synoptic gauge records of Iran 1998-2006. Many other studies (e.g. Alijanian et al., 2017; Azizi et al., 2016; Darand et al., 2017; Azizian and Ramezani Etedali, 2019; Darand and Khandu, 2020; Hosseini-Moghari and Tang, 2020; Ababaei and Etedali, 2021; S. M. Hosseini-Moghari et al., 2018; Katiraie-Boroujerdy et al., 2017, 2013; Katiraie Boroujerdy, 2013; Moazami et al., 2016, 2013; Raziei and Sotoudeh, 2017; Sharifi et al., 2016; Ghajarnia et al., 2018) have since evaluated different sets of global precipitation products against in-situ observations from Iran and compared the performance of these products in different temporal extents and at varying temporal and spatial scales. Many of these studies have found that most products are more efficient in the Zagros mountains and southern Iran than in coastal regions in the north, where all products have shown poor performance (Alijanian et al., 2017; Katiraie-

82 Boroujerdy et al., 2013; Moazami et al., 2016; Raziei and Sotoudeh, 2017; Sharifi et al., 2016).

83 Some studies have suggested that gauge-adjusted TRMM Multi-satellite Precipitation Analysis

84 (TMPA) (Huffman et al., 2007) and fully ground-based products such as Global Precipitation

85 Climatology Centre (GPCC) (Schneider et al., 2011) and Asian Precipitation-Highly-Resolved

86 Observational Data Integration Towards Evaluation (APHRODITE) (Yatagai et al., 2012) may be

87 more efficient than other products in terms of different statistical and categorical metrics across

88 the whole country (Azizi et al., 2016; Darand and Khandu, 2020; S.-M. Hosseini-Moghari et al.,

89 2018; P. S. Katiraie-Boroujerdy et al., 2017; Moazami et al., 2013). More recently, Fallah et al.

90 (2020) evaluated different precipitation products using data for Karun basin and found that

91 GPCCV8.0 was more efficient than other products in this basin. A wide range of precipitation

92 products was evaluated using data for Karkheh basin by Mosaffa et al. (2020), who concluded that

93 PERSIANN-CDR and Soil Moisture (SM) to Rain (SM2RAIN) were more efficient than other

94 products for daily precipitation estimations. These basin-scale studies and two other studies in Iran

95 (Fallah et al., 2020; Mosaffa et al., 2020) provided a better basis for choosing a good source of

96 precipitation estimates. However, there is still considerable uncertainty regarding various aspects

97 of precipitation products at different spatial and temporal scales in Karun and Karkheh basins. A

98 growing body of literature has focused on a limited number of global precipitation products, and

99 the periods and time scales of comparisons differ between studies. Another key difference between

100 existing studies is that different observational gauge datasets have been used as reference data,

101 such as those from Iran Meteorological Organization (IRIMO) and Iran Water Management

102 Research Institute (TAMAB). Thus previous studies of Iran, and particularly of Karun and

103 Karkheh basins, have still shortcomings, especially in the evaluation approaches and reference

104 datasets used, which makes comparison of results difficult. For instance, Mosaffa et al. (2020)

only used 26 rain gauges in Karkheh basin for daily assessments and Fallah et al. (2020) only focused on monthly evaluations, with limited numbers of metrics. Therefore, it is not feasible to draw conclusions for the specific region of interest from these studies.

Karun and Karkheh basins, the food baskets of Iran, contain the largest rivers in the country (Karun and Karkheh rivers). These two basins are critically important in terms of agricultural production, water resources, and energy supply (Ahmad and Giordano, 2010; Hishinuma et al., 2014; Marjanizadeh et al., 2010). In recent years, the occurrence of multi-year droughts and devastating floods caused by climate change and different anthropogenic interventions in the basins has made the limited water resources in the region even more vulnerable (Afkhami et al., 2007; Peyravi et al., 2019; Vaghefi et al., 2019). Precipitation is one of the main factors influencing the hydro-climatology of these two large basins, and therefore spatio-temporal analysis of precipitation is highly important from various aspects, such as quantifying hydrological patterns of the biggest rivers in Iran, inflow to multiple parallel or series dams, agricultural demands, and environmental supplies. In addition, it is important to note that the observational rain-gauge network in Iran suffers from uncertainties and measurement inconsistencies (Ghajarnia et al., 2014). Most previous studies have only used synoptic station records (as they are the most accurate rain gauges in Iran) and have neglected data from other rain gauges, such as those used by TAMAB, but synoptic stations are mostly located at low altitudes and do not sample higher elevations (which TAMAB stations do). Therefore, there is a need for a comprehensive study of Karun and Karkheh basins, considering a more complete set of in-situ rain gauges and including both synoptic stations and TAMAB stations with better coverage of higher altitudes, when evaluating the performance of the most commonly used global precipitation products in these basins.

The aim of this study was to evaluate the performance of 14 common and well-known global precipitation products: PERSIANN, PERSIANN-CDR, PERSIANN-CCS, CMORPH-RAWV1.0, CMORPH-BLDV1.0, CMORPH-CRTV1.0, TMPA-3B42V7.0, TMPA-3B42RTV7.0, ERA5-Land, MERRA-2, JRA-55, PGFV2.0, MSWEPV2.0, and CHIRPSV2.0 against data from the domestic rain gauge network in Karun and Karkheh basins. Product performance was analyzed using daily precipitation data 2003-2012 (and monthly data aggregated from daily observations), as described in section 2. The evaluation was performed using different statistical and categorical measures, which are also described in section 2. Results and discussion are presented in section 3, followed by a summary and conclusions in section 4.

2. Material and Methods

2.1. Study area

The study area lies between latitude 29°-35°N and longitude 46°-52° E and encompasses Karkheh and Karun basins, through which two of the largest rivers in Iran flow (Fig. 1). Karkheh and Karun basin occupy an area of 51,000 and 67,000 km², respectively, and long-term average streamflow is around 170 and 590 m³/s, respectively (Khazaei, 2021). The Zagros mountain range makes these basins among the most complex terrain in Iran, with their average elevation increasing drastically from 0 to 3916 m above sea level from north to south. Mean annual precipitation in Karkheh basin is around 450 mm/year, with a spatial variation range from 150 mm/year on arid low-elevation plains to 750 mm/year in highlands (Choubin et al., 2019). Mean annual precipitation in Karun basin is 632 mm/year, with larger spatial variability of 153 mm/year in arid southern lowlands to >2000 mm/year in mountainous areas (Fallah et al., 2020).

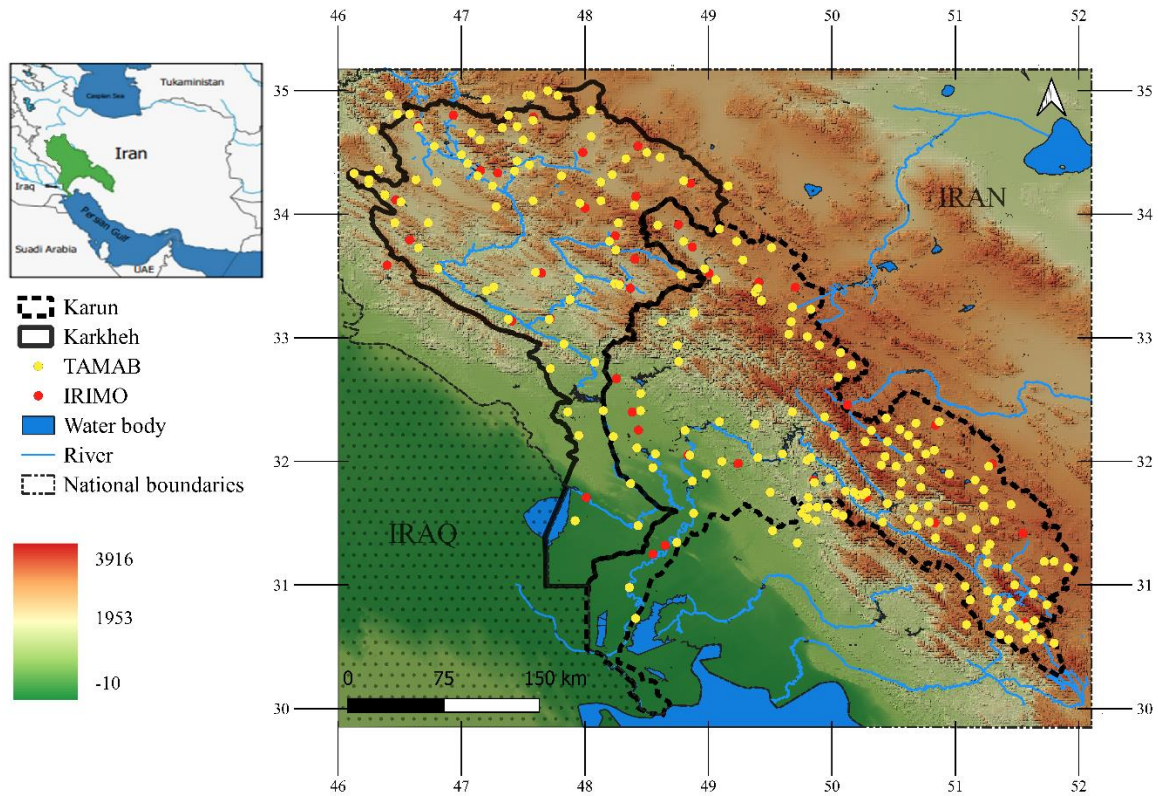


Fig. 1. Topographical map of the Iran showing Karkheh and Karun basins in the south-western plains area.
Rain gauge stations used in the reference dataset are shown as yellow dots.

2.2. Reference data

Rain gauge data provided by IRIMO and TAMAB were used as the reference dataset. Daily data from a total of 254 gauge stations within a 10-year period (2003-2012) were used to evaluate the performance of different global precipitation products. Figure 1 shows the spatial distribution of the rain gauges across Karkheh and Karun basins.

2.3. Global precipitation products

Fourteen global precipitation estimation products with different temporal and spatial resolution were chosen, and classified as reanalysis, satellite-based, and multi-source precipitation products (Table 1).

2.3.1. Reanalysis precipitation products

Reanalysis datasets provide a spatially complete and temporally coherent time series of data for different global atmospheric variables by benefiting from three main components: data assimilation approaches, forecasting models, and different input observations (Dee et al., 2011). Due to the lack of globally consistent observational data, climate reanalysis products are used as an alternative in a wide range of earth science studies (Qian et al., 2006). In this study, we used precipitation data from three reanalysis products: the European Center for Medium-range Weather Forecast ReAnalysis (ECMWF) 5th Generation-Land (ERA5-Land) (Hersbach et al., 2020), Japanese 55-year Reanalysis (JRA-55) (Kobayashi et al., 2015), and Modern-Era Retrospective analysis for Research and Applications, Version 2 (MERRA-2) (Rienecker et al., 2011). ERA5-Land provides a consistent view of the evolution of land variables over many decades at higher spatial and temporal resolution compared with ERA5, which was developed by replaying the land component of the ECMWF ERA5 climate reanalysis (Sabater and Data, 2019). Spanning 1950-present time, ERA5-Land is one of the longest and finest reanalysis products, with temporal resolution of one hour and spatial native resolution of 9 km (Hersbach et al., 2020). JRA-55, the second reanalysis product launched by Japan Meteorological Agency, extensively improved the Japanese 25-year Reanalysis product (JRA-25) (Onogi et al., 2007). JRA-55 addresses issues identified with the previous product and produces relevant detailed climate data, especially for climate change studies and assessing multidecadal variabilities (Kobayashi et al., 2015). The daily JRA-55 reanalysis product with spatial resolution of $1.25^{\circ} \times 1.25^{\circ}$ covers the entire globe (Kobayashi et al., 2015). MERRA-2 is NASA's second-generation reanalysis product, spanning 1979 to the present. MERRA-2 utilizes a recent version of the Goddard Earth Observing System

Model, Version 5 (GEOS-5) data assimilation system. It covers the whole globe with high spatial resolution of $0.5^{\circ} \times 0.67^{\circ}$ and hourly time steps (Rienecker et al., 2011).

2.3.2. Satellite-based precipitation products

Satellite-based precipitation estimates offer an alternative way to monitor precipitation at global scale, compared with ground-based observations. Considering the high variability of precipitation in time and space, satellites can provide valuable information for estimating precipitation with suitable spatial and temporal resolution (Kidd and Huffman, 2011). For this study, we selected four widely used satellite-based products: TRMM multisatellite precipitation analysis, near-real-time (3B42RT) Version 7 (TMPA-3B42RTV7.0), Climate Prediction Center MORPHing RAW Version 1 (CMORPH-RAWV1.0), Precipitation Estimation from Remotely Sensed Information using Artificial Neural Networks (PERSIANN), and PERSIANN-Cloud Classification System (PERSIANN-CCS). By using various meteorological satellites around the world, TMPA provides precipitation estimates at $0.25^{\circ} \times 0.25^{\circ}$ spatial resolution (covering 50°N to 50°S), at 3-hourly time scales, for 1998-2016 (Huffman et al., 2007). TMPA-3B42RTV7.0 is the near real-time (with latency of 7 h from the observation time) version of TMPA products. The satellite-based PERSIANN product is designed to produce global precipitation estimations at $0.25 \times 0.25^{\circ}$ spatial resolution using an artificial neural network. In order to generate 30-minute rainfall estimate, PERSIANN utilizes the global infrared (IR) information from geosynchronous satellites (GOES-8, GOES-10, GMS-5, Metsat-6, and Metsat-7) provided by the National Oceanic and Atmospheric Administration (NOAA) Climate Prediction Center (CPC) and then aggregates these estimates into 6-h rainfall (Hsu et al., 1997; Sorooshian et al., 2000). PERSIANN-CCS is a successor of the PERSIANN product that also benefits from satellite information on cloud attributes and further incorporates them into the rainfall estimation relationships (Hong et al., 2004). In comparison with

PERSIANN, the CCS version has finer spatial resolution ($0.04^{\circ} \times 0.04^{\circ}$), covering 60°N - 60°S for 2004-present time at different temporal scales. CMORPH-RAWV1.0 is a near-real-time product developed by NOAA. It is based on low-orbital satellite passive microwave (PMW) sensors with IR information used to interpolate between successive PMW-derived rainfall intensity fields (Joyce et al., 2004). The primary and reprocessed versions of CMORPH are called Version 0.x and Version 1, respectively.

2.3.3. Multi-source precipitation products

Different multi-source precipitation products were developed due to the short period and uncertainties of precipitation estimation from satellite-based precipitation products. These multi-source precipitation products are a combination of two or more precipitation estimations from various sources. In this study, we used seven high-resolution multi-source products, namely CMORPH bias-corrected Version 1 (CMORPH-CRTV1.0), CMORPH satellite-gauge merged Version 1 (CMORPH-BLDV1.0), Climate Hazards Group InfraRed Precipitation with Station V2 (CHIRPSV2.0), PERSIANN-Climate Data Record (PERSIANN-CDR), TRMM multisatellite precipitation analysis: research-grade (3B42) Version 7 (TMPA-3B42V7.0), Multi-Source Weighted Ensemble Precipitation Version 2 (MSWEPV2.0), and Princeton Global Forcings Version 2 (PGFV2.0). CMORPH-V1.0 contains three different precipitation products: (i) CMORPH-RAW (introduced earlier), (ii) CMORPH-CRT, the bias-corrected version using the probability density function (PDF)-matching bias-removal technique on CMORPH-RAW, and (iii) CMORPH-BLD merged product, generated by calibrating CMORPH-RAW estimates with in-situ data and using optional interpolation technique (Joyce et al., 2004). CHIRPSV2.0 is another reliable, up-to-date product for many early warning objectives that covers areas exceeding 50°N - 50°S . It provides precipitation estimates in the period 1981-present time and combines high-

228 resolution satellite imagery ($0.05^{\circ} \times 0.05^{\circ}$) with data from in-situ stations (Funk et al., 2015).
229 PERSIANN-CDR is also based on the original PERSIANN algorithm using Gridded Satellite B1
230 (GridSat-B1) infrared data and adjusted using the Global Precipitation Climatology Project
231 (GPCP) monthly product (Ashouri et al., 2015). This product was created for extreme daily
232 precipitation events and climate studies that require data for more than 30 years. PERSIANN-CDR
233 is available in high spatial resolution ($0.25^{\circ} \times 25^{\circ}$), covering 60N-60S for 1983-present time (with
234 a 3-month time delay). TMPA-3B42V7.0 is the research product of TMPA, calibrated via gauge
235 data and incorporating different sensor calibrations and additional post-processing. It is available
236 in $0.25^{\circ} \times 0.25^{\circ}$ spatial resolution and covers 50°N to 50°S for 2000-2016 (Huffman et al., 2007;
237 Liu, 2015). MSWEPV2.0, recently developed by Beck et al. (2019), is a global precipitation
238 product with temporal and spatial resolution of 3 hours and 0.1° for 1979-2020. The exceptional
239 feature of MSWEPV2.0 is that it combines in-situ, satellite, and reanalysis data to provide high-
240 quality global precipitation estimates. PGF is another global precipitation product that combines
241 several sources, including in-situ, satellite, and reanalysis data, disaggregating them in time and
242 space. It is available in 3-hour to monthly temporal scale with 1.0° , 0.5° , and 0.25° spatial
243 resolution (Sheffield et al., 2006).

Table 1. Main characteristics and references for different precipitation products used in this study. In the data source column, S, R, and G represents satellite, reanalysis, and gauge information, respectively.

<i>Name</i>	<i>Details</i>	<i>Temporal coverage</i>	<i>Temporal resolution</i>	<i>Spatial coverage</i>	<i>Spatial resolution</i>	<i>Data source</i>	<i>Reference</i>
Era5- Land	European Center for Medium-range Weather Forecast ReAnalysis 5th Generation- land	1950-present	Hourly	Global	0.1° × 0.1°	R	(Hersbach et al., 2020)
MERRA-2	Modern-Era Retrospective analysis for Research and Applications, V2	1980-present	Hourly	Global	0.5° × 0.67°	R+G+S	(Rienecker et al., 2011)
JRA-55	Japanese 55-year Reanalysis	1959-present	3 h	Global	1.25° × 1.25°	R	(Kobayashi et al., 2015)
TMPA-3B42RTV7.0	TRMM multisatellite precipitation analysis: near-real-time (3B42RT) V7	1998–2016	3 h	60°N–60°S	0.25° × 0.25°	S+G	(Huffman et al., 2007)
TMPA-3B42V7.0	TRMM multisatellite precipitation analysis: research-grade (3B42) V7	2000-2016	3 h	50°N–50°S	0.25° × 0.25°	S+G	(Huffman et al., 2007)
CMORPH-RAW V1.0	Climate Prediction Center MORPHing raw V1	1998-present	3 h	60°N–60°S	0.25° × 0.25°	S	(Joyce et al., 2004)
CMORPH-CRT V1.0	CMORPH bias corrected V1	1998-present	3 h	60°N–60°S	0.25° × 0.25°	S+G	(Xie et al., 2017)
CMORPH-BLD V1.0	CMORPH satellite-gauge merged V1	1998-present	Daily	60°N–60°S	0.25° × 0.25°	S+G	
PERSIANN	Precipitation Estimates from Remotely Sensed Information using Artificial Neural Network	2000-present	Hourly	60°N–60°S	0.25° × 0.25°	S	(Sorooshian et al., 2000)
PERSIANN-CCS	PERSIANN-Cloud Classification System	2003-present	Hourly	60°N–60°S	0.04° × 0.04°	S	(Hong et al., 2004)
PERSIANN-CDR	Precipitation Estimates from Remotely Sensed Information using Artificial Neural Network and Climate Data Record	1983-present	Daily	60°N–60°S	0.25° × 0.25°	S+G	(Ashouri et al., 2015)
MSWEP V2.0	Multi-Source Weighted Ensemble Precipitation v.2.2	1979-present	3 h	Global	0.25° × 0.25°	R+G+S	(Beck et al., 2019b)
PGFV2.0	Princeton Global Forcings V2	1901-2012	3 h	Global	0.25° × 0.25°	R+G+S	(Sheffield et al., 2006)
CHIRPSV2.0	Climate Hazards Group InfraRed Precipitation with Station V2	1981-present	Daily	50°N–50°S	0.25° × 0.25°	S+G	(Funk et al., 2015)

2.4. Evaluation approach

Several steps were taken to evaluate the performance of the global precipitation products. Initially, long-term time series of the precipitation estimates from all 14 global products and observed precipitation at rain gauge stations were collected and preprocessed by reformatting the data to

prepare them for performance evaluations, tasks carried out using Climate Data Operator (CDO) (Schulzweida, 2019). Various statistical metrics were then used to characterize model behaviors and quantify their associated uncertainties and errors in precipitation estimation. This step was carried out using Climate Data Tools (CDT) and HydroGOF packages in the R programming environment (Zambrano-Bigiarini, 2014). The error at different spatial and temporal scales for global precipitation products was computed and illustrated using various visualization techniques. The most common methods for error determination are continuous statistical parameters and metrics based on contingency tables. The primary purpose of this study was to evaluate the performance of precipitation products in daily and monthly time steps. However, annual time series and mean annual precipitation for precipitation products were also examined in the study area.

2.4.1. Continuous statistical indices

Kling-Gupta efficiency (KGE) was used to study the accuracy of precipitation estimations by different products. KGE combines correlation coefficient (r), bias (β), and variability component (γ) as (Gupta et al., 2009; Kling et al., 2012):

$$KGE = 1 - \sqrt{(r-1)^2 + (\beta-1)^2 + (\gamma-1)^2} \quad (1)$$

where r denotes the Pearson correlation coefficient (hereafter CC, see Eq. (2)), β is the bias component defined as the ratio between average observed and estimated precipitation values (Eq. (3)), and γ represents the variability and is defined as the ratio of the estimated and observed coefficients of variations (eq. (4)). In the following equations, μ_O and μ_E are the average precipitation values in the observational and estimated times series, respectively, while σ_O and σ_E show the standard deviations of observations and estimations. n is the number of records in

the time series with valid observed or estimated data (number of records excluding the no-data values in the time series). O_i and E_i also denote the observational and estimated data at date i in the time series. KGE, r , β , and γ all have their optimum value at unity.

$$r = \frac{1}{n} \sum_{i=1}^n \frac{(O_i - \mu_O) * (E_i - \mu_E)}{\sigma_O * \sigma_E} \quad (2)$$

$$\beta = \frac{\mu_E}{\mu_O} \quad (3)$$

$$\gamma = \frac{\frac{\sigma_E}{\mu_E}}{\frac{\sigma_O}{\mu_O}} \quad (4)$$

2.4.2. Categorical statistical indices

Categorical statistics measure the agreement between estimated and observed occurrence of events. In this study, the contingency table shown in Table 2 was used to define dichotomous estimations and calculate contingency table indices (Wilks, 2011). A dichotomous estimate determines the occurrence and non-occurrence of rainfall as "Yes" and "No" events, respectively. In order to detect "Yes" and "No" precipitation events, a threshold needs to be specified. In this study the threshold was set at 1 mm/day, based on similar assumptions in previous studies (e.g., Ghajarnia et al., 2015; Zhang et al., 2010). In the contingency table, a Hit event indicates the condition in which both observational and estimated datasets agree on the occurrence of precipitation, while a False Alarm (FA) shows that the precipitation event estimated by the model has not occurred in reality and is not a precipitation event in the observational dataset (Wilks, 2011). Similarly, a Miss refers to an event recorded in the reference observation dataset but missed by the global precipitation estimation product, while a Correct Negative (CN) indicates that both observational dataset and estimation products have reported a No rainfall event (Wilks, 2011). Based on the time series of dichotomous conditions and the number of Hit, FA, Miss, and CN

variables, different indicators are defined and can be calculated to evaluate the performance of different global models in estimation of precipitation occurrence (see Ebert et al. (2007) for more details). In this study, we used three indicators, Probability of Detection (POD), False Alarm Ratio (FAR), and Heidke Skill Score (HSS), to measure the association between precipitation products and observed rainfall occurrences. POD determines the ratio of correctly identified rainfall events by the precipitation product to the total number of real rain events based on the observational dataset (perfect score = 1). FAR shows the ratio of the total number of false rainfall identifications by the model to the total number of estimated Yes rainfall events by the global precipitation product (perfect score = 0). HSS also measures the overall ability of precipitation estimation product in capturing the occurrence of precipitation events (perfect score = 1). Equations (5) to (7) were used to calculate POD, FAR, and HSS based on the dichotomous statistics according to Table 2.

Table 2. Contingency table for determining dichotomous (Yes/No) estimations and calculation of categorical indices

		Observation	
		Yes	No
Estimation	Yes	a	b
	No	c	d

$$\text{POD} = \frac{a}{a + c} \quad (5)$$

$$\text{FAR} = \frac{b}{b + a} \quad (6)$$

$$\text{HSS} = \frac{2(ad-bc)}{[(a+c)(c+d)+(a+b)(b+d)]} \quad (7)$$

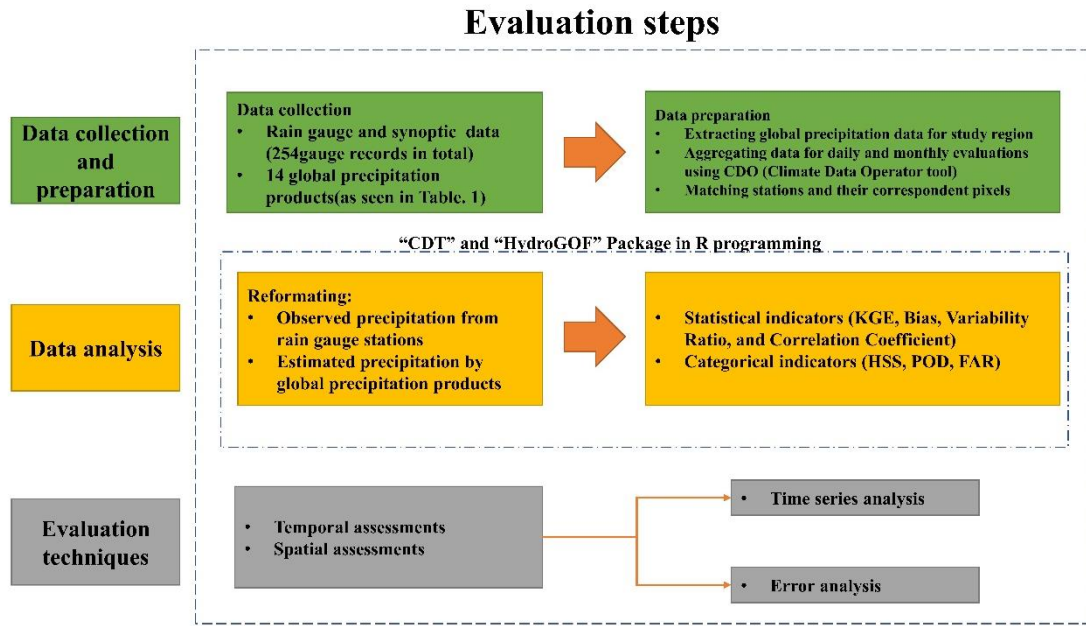


Fig. 2. General framework for data preparation and performance evaluation used in this study.

3. Results and Discussion

3.1. Overall performance of models at annual and monthly time scales

The mean annual precipitation (MAP) map for Karun and Karkheh basins based on all gridded precipitation products and interpolated gauge records during the period 2003-2012 is shown in Figure 3. MAP in gauge records varied from 134 to 1384 mm/year across the basins and increased from the northwestern lowlands of Karkheh basin to the southeastern highlands of Karun. This indicates that there is a spatial pattern and relationship between MAP and elevation, with high-altitude areas receiving higher amounts of annual precipitation. The terrain barrier effect leads to high precipitation rates over mountainous regions in the Zagros chain, which are a bulky feature with continuous ridge lines. In these areas, the precipitation rate is more affected by elevation changes.

Overall, visual comparison of the MAP patterns for the basins showed that the main spatial patterns produced by TMPA-3B42V7.0 were the closest to the observations, followed by ERA5-Land and MERRA-2 with slight overestimations and CHIRPSV2.0 with a slight underestimation relative to the observational spatial pattern (Fig. 3). The PERSIANN family seemed to be less successful in capturing the spatial pattern of MAP in general, but PERSIANN-CCS performed better than the others, with more accurate estimations of MAP in the mountainous areas of Karun basin, while PERSIANN significantly underestimated MAP values in the highlands. CMORPH-CRT and CMORPH-BLD (adjusted versions) both improved estimations of CMORPH-RAW (non-adjusted version), but still underestimated MAP in the study area and did not correctly capture the increasing spatial pattern from lowlands to highlands. PERSIANN, MSWEPV2.0, and PGFV2.0 simulated the observed spatial pattern of MAP in declining order and all largely underestimated precipitation in the study area. JRA-55 also showed relatively poor performance in capturing the MAP spatial pattern, considering its coarser spatial resolution compared with other products.

Due to complex topography and the particular climate system over the study region, affected by coast proximity to the west and high mountainous ranges in the central lands, precipitation estimation was not an easy task for the global products studied. The highest and lowest MAP value among all products was produced by ERA5-Land and CMORPH-CRTV1.0, respectively, with recorded precipitation of up to 1500 and below 40 mm/year, respectively, in central areas of Karun basin (and southwestern parts of Karkheh basin). As found previously by Javanmard et al. (2010) and Darand et al. (2017), TMPA-3B42V7.0 showed relatively good performance in capturing annual precipitation in the study region, with only slight underestimation.

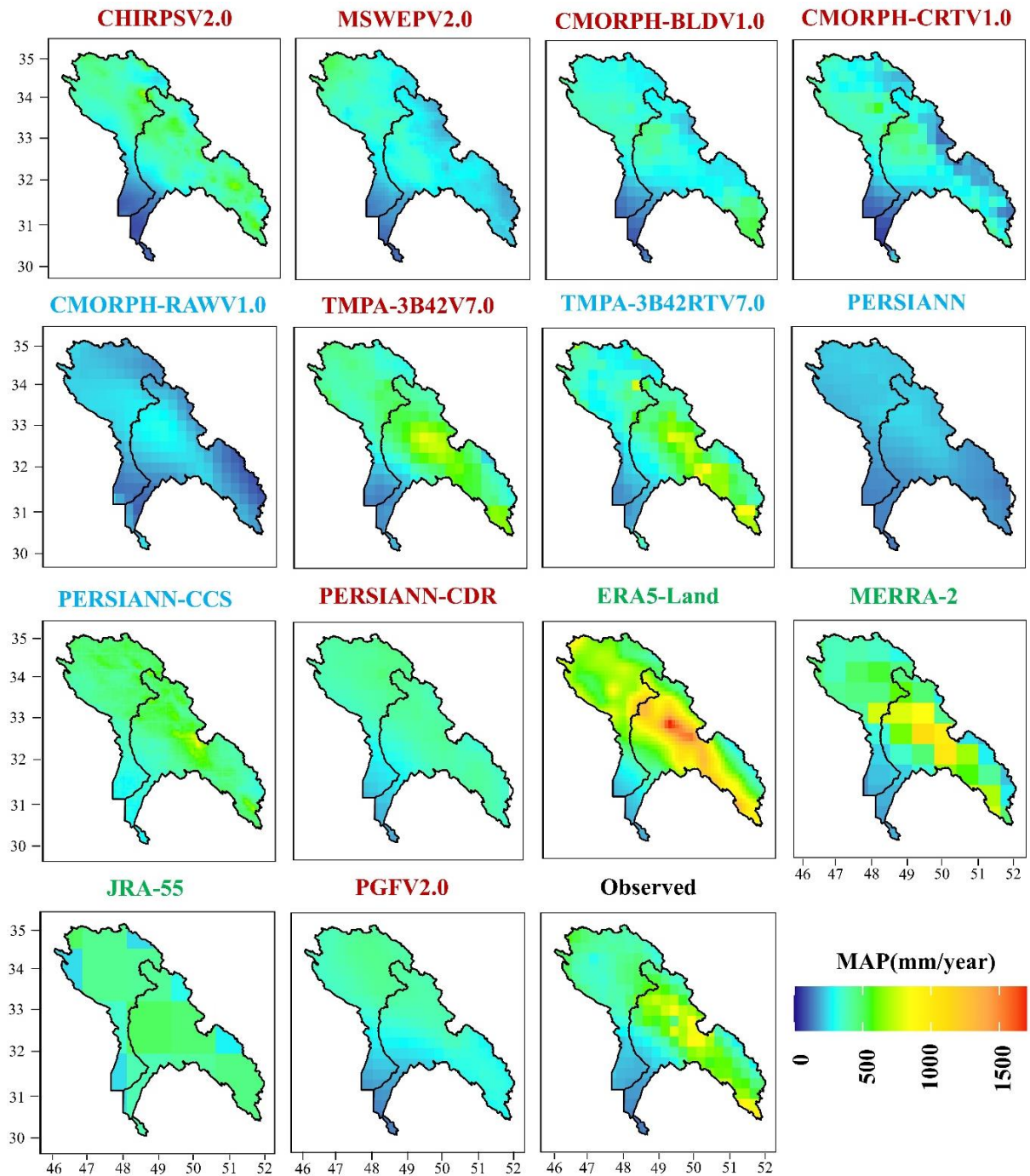


Fig. 3. Mean annual precipitation (MAP) 2003-2012 retrieved from all products at their original grid sizes.
Blue, red, and green indicates satellite-based, multi-source, and reanalysis precipitation products,
respectively.

Figures 4 and 5 show the temporal variation in annual and monthly precipitation time series 2004-2012, measured at the rain gauge stations and estimated by different precipitation products. The bias-adjusted products MERRA-2, MSWEPV2.0, CMORPH-CRTV1.0, CMORPH-BLDV1.0, TMPA3B42V7.0, PERSIANN-CDR, and PGFV2.0, but not CHIRPSV2.0, showed almost similar trends throughout the study period (except for 2004) with annual variation close to that in observations (Fig. 4). Although the performance of some unadjusted products (i.e., JRA-55, PERSIANN-CCS, and ERA5-Land) was not acceptable when compared against the observational data, their performance slightly improved after 2008. ERA5-Land made the highest overestimation of all products, while PERSIANN and CMORPH-RAWV1.0 made the highest underestimation on an annual basis (Fig. 4). The temporal trend of precipitation at monthly scale showed relatively better performance of TMPA-3B42V7.0 and poor estimation by PERSIANN-CDR, PERSIANN-CCS, PERSIANN, and CHIRPSV2.0 (Fig. 5). Other products were capable overall of detecting the general trend in observed precipitation with reasonable accuracy and slight over- or under-estimation. All products except ERA5-Land tended to underestimate observed precipitation over the study area, both at annual and monthly time scales. The results obtained from time series analysis are consistent with the results from mean annual precipitation maps (see Fig. 3), which showed great overestimation by ERA5-Land across mountainous regions and better results for TMPA-3B42V7.0 overall. Although both PERSIANN-CDR and TMPA-3B42V7.0 utilized the same observational precipitation data source (GPCP; Adler et al., 2003; Huffman et al., 2007) to improve their estimations, the calibration procedure used in TMPA-3B42V7.0 seemed to be more efficient than PERSIANN-CDR and provided TMPA-3B42V7.0 with better accuracy for the study area in terms of the spatial variation in MAP and monthly and annual estimations.

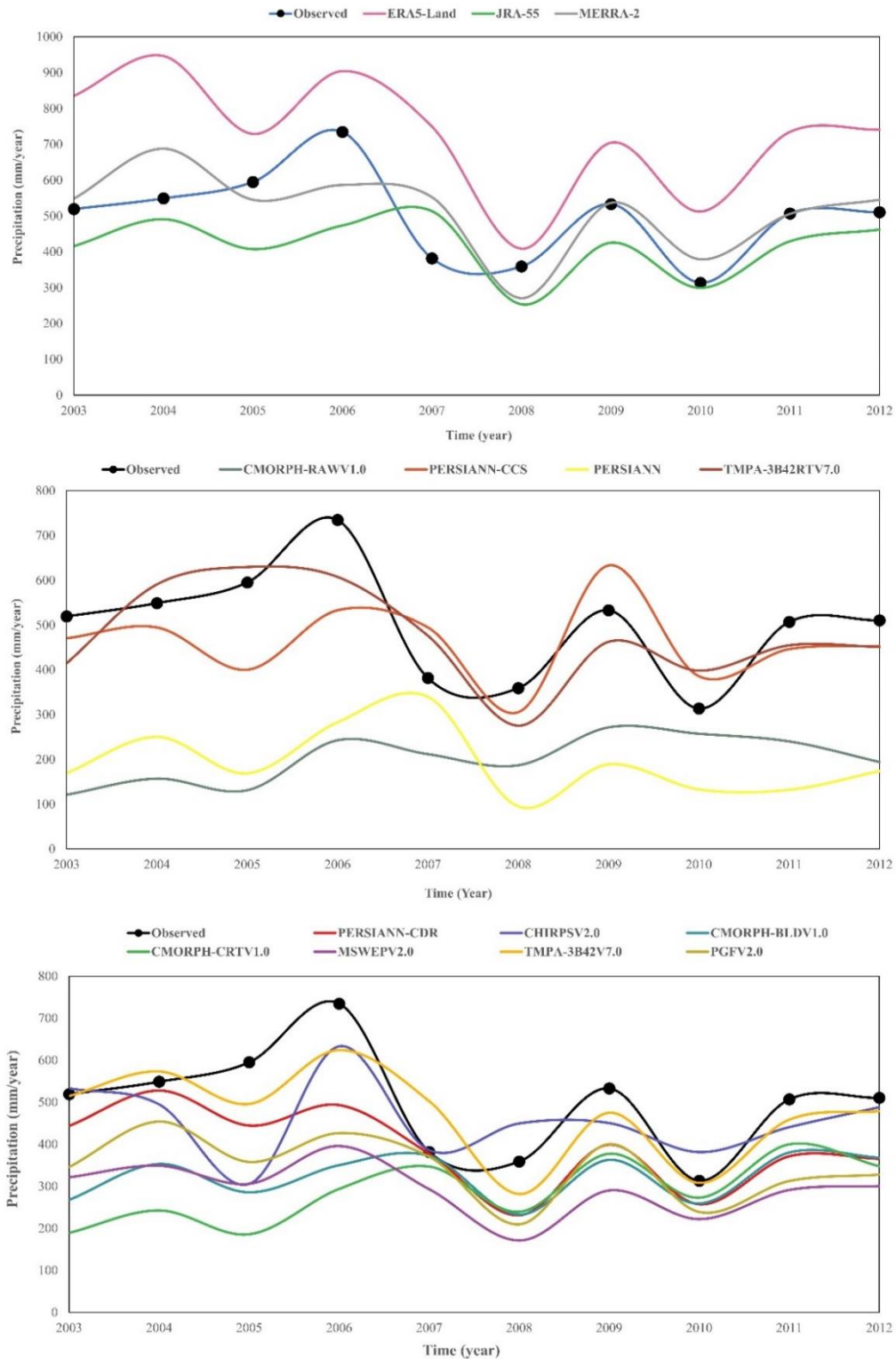


Fig. 4. Mean annual precipitation in the study area based on the observational dataset and estimations made by global precipitation products. Reanalysis, satellite-based, and multi-source precipitation products are presented in the top, middle, and bottom panel, respectively.

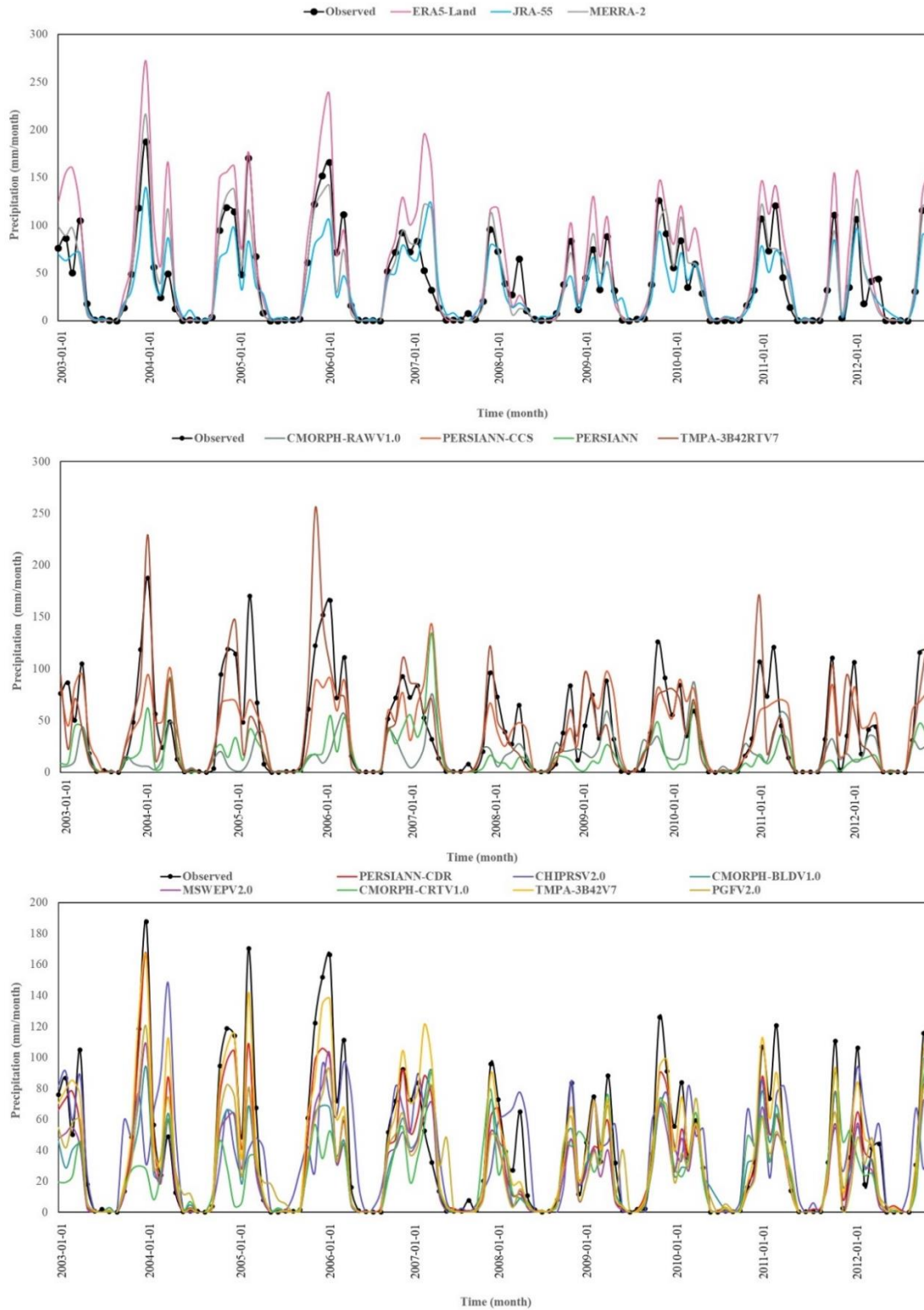


Fig. 5. Mean monthly precipitation in the study area based on the observational dataset and estimations made by global precipitation products. Reanalysis, satellite-based, and multi-source precipitation products are presented in the top, middle, and bottom panel, respectively.

3.2. Statistical error in global precipitation product estimates at daily scale

The performance of all 14 precipitation products at daily time steps, based on the KGE error index and its related components, is compared and evaluated in Figure 6. All products showed relatively poor accuracy, with negative KGE value for PERSIANN-CDR, CMORPH-RAWV1.0, PERSIANN, and CHIRPSV2.0. All products had $KGE < 0.4$, but MERRA-2, with approximately $KGE = 0.4$, performed better than all other products (Fig. 6). Overall, the bias-adjusted products (i.e., TMPA-3B42V7.0, CMORPH-BLDV1.0, and CMORPH-CRTV1.0) outperformed the unadjusted products (i.e., CMORPH-RAWV1.0 and TMPA-3B42RTV7.0) in terms of KGE (except for PERSIANN-CDR, which was the most inaccurate product).

Given the poor performance of PERSIANN-CDR, CMORPH-RAWV1.0, PERSIANN, and CHIRPSV2.0 (Fig. 6), caution is needed in water-related applications of these products at daily time scale in the study area.

The CC, bias, and variability ratio values revealed interesting details on the performance of different products, leading to their general KGE values (Fig. 6). Based on CC, ERA5-Land performed best among all products ($CC > 0.6$), but its high bias value (> 1.5) led to low overall KGE value (0.22) for the study area. In terms of bias, PERSIANN, CMORPH-RAWV1.0, CMORPH-CRTV1.0, CMORPH-BLDV1.0, MSWEPV2.0, and PGFV2.0 underestimated precipitation to some extent (bias < 0.7) while ERA5-Land was the only product with clear overestimation at daily time scale, similar to the annual and monthly results in Figures 4 and 5. In terms of variability ratio, MERRA-2, TMPA-3B42V7.0, and PGFV2.0 with their higher KGE values also displayed variability ratio values closer to one, while CMORPH-RAWV1.0 and PERSIANN-CDR, with negative KGE values, tended to underestimate the variability in the observed precipitation dataset across the study area and at daily scale.

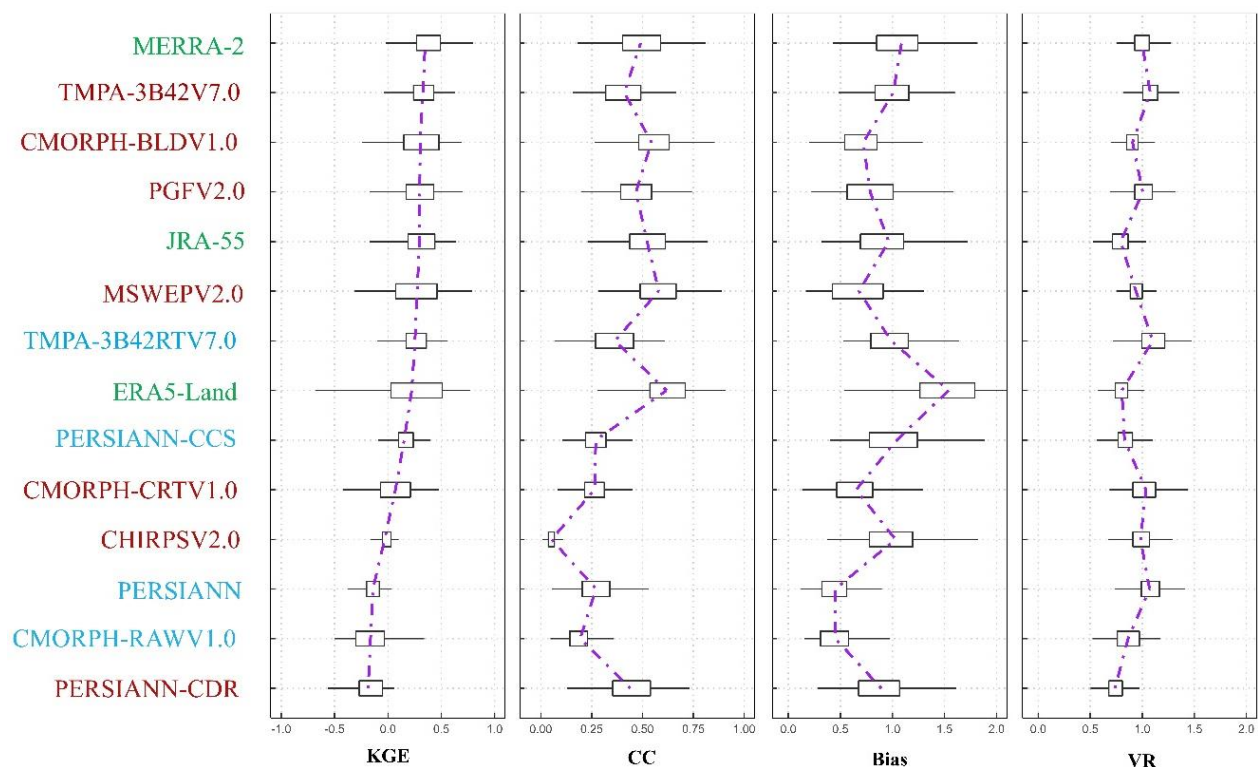


Fig. 6. Box plots of Kling-Gupta Efficiency (KGE) index and its related components correlation coefficient (CC), bias, and variability ratio (VR), calculated for all precipitation products at daily time steps throughout 2003-2012. The products are arranged in order of highest (top) to lowest (bottom) average KGE.

Figure 7 shows the spatial distribution of KGE index for different products that gave scores varying from very low to high for the study area. The KGE scores ranged from around -1.65 for PERSIANN-CDR to approximately 0.8 for MERRA-2 across various regions, indicating varying performance of the products in matching reference precipitation at daily time steps. Considering the spatial distribution of KGE, it is noteworthy that CHIRPSV2.0, CMORPH-RAWV1.0, CMORPH-CRTV1.0, and all products in the PERSIANN family showed lower accuracy, with $KGE < 0.3$ in most regions. However, MERRA-2, MSWEPV2.0, CMORPH-BLDV1.0, ERA5-Land, and PGFV2.0 outperformed other products and provided better daily estimations at different locations around the study area. The results also indicated that using gauge data was effective for products in the CMORPH and TMPA families, while there was no significance improvement for

the bias-adjusted version of PERSIANN (i.e., PERSIANN-CDR) (Fig. 7). CMORPH-BLDV1.0, which benefits from a proper calibration procedure, is PMW-based and the distinction between snowfall and precipitation over mountainous regions is well captured by this product. The IR-based products (i.e., CHIRPSV2.0, PERSIANN, PERSIANN-CDR, and PERSIANN-CCS) did not perform well for mountainous regions (Fig. 7). Previous studies suggest that IR-based products have limitations in estimating orographic rain events over complex terrain (Derin et al., 2016; Shen et al., 2020; Tong et al., 2014; Yong et al., 2015), as confirmed by our findings (Fig. 7). The low KGE value of MSWEPV2.0 for the Zagros mountains might result from associated uncertainty from all precipitation products for this region, since it merges multiple precipitation products to produce its final estimations (Beck et al., 2019b). Overall, the findings and patterns obtained (Fig. 7) indicated that the majority of global precipitation products were ineffective for daily hydrological applications across the study area. Due to the vital importance of Karun and Karkheh basins for water resources and hydrology in Iran, use of global daily precipitation products after proper bias adjustment and enhancement of the estimations is indicated.

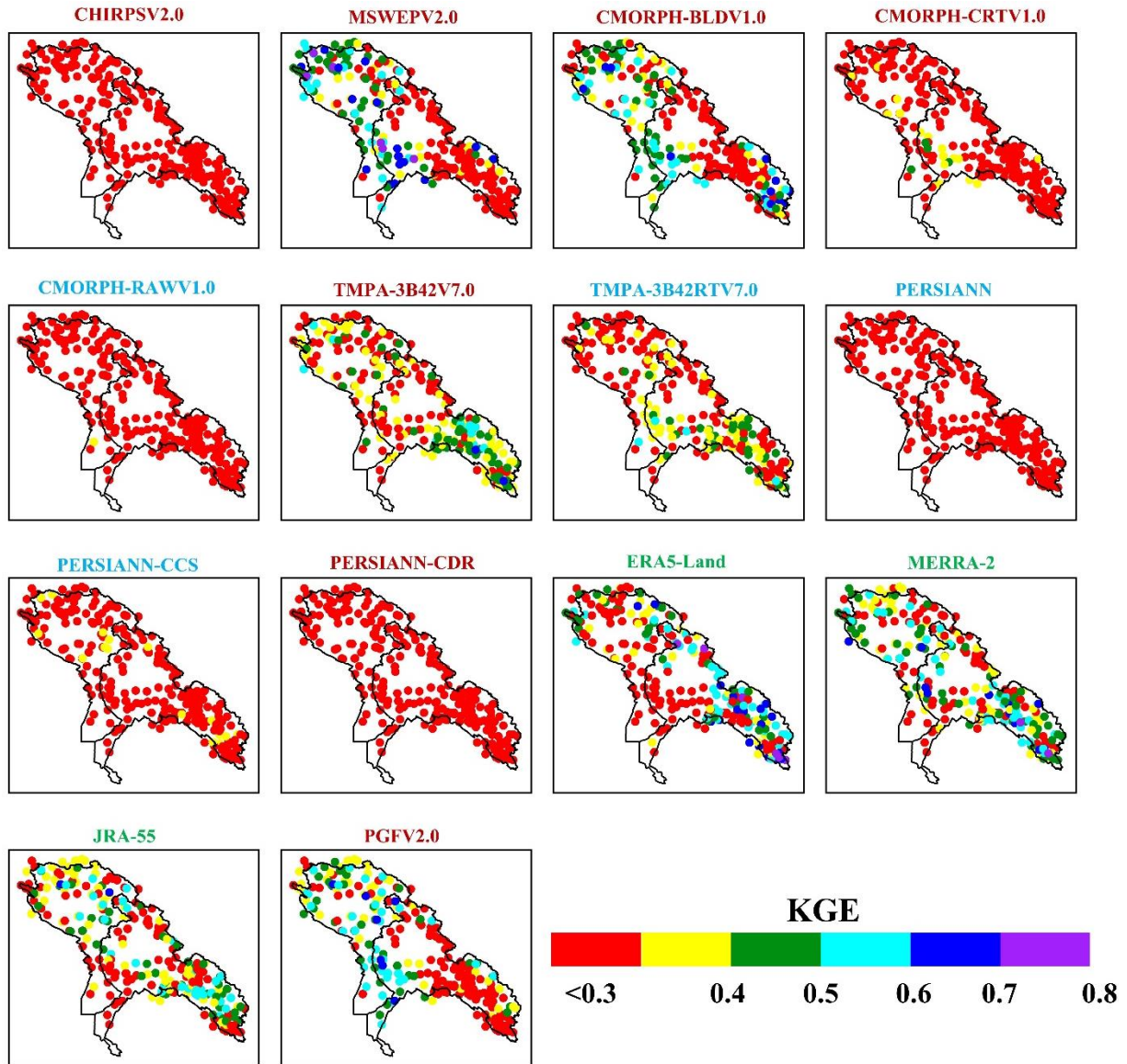


Fig. 7. Spatial distribution of Kling-Gupta Efficiency (KGE) index for the different global precipitation products at daily time step. Blue, red, and green indicates satellite-based, multi-source, and reanalysis precipitation products, respectively.

Full CC, bias, and variability ratio maps are provided in Supplementary Information (Figs. S1-3). Fig. S1 compared the spatial patterns of the CC maps between different global precipitation products at daily time scale. In general, MSWEPV2.0, ERA5-Land, and CMORPH-BLDV1.0 estimates were well correlated with the gauge precipitation data, especially in the southeastern

region of Karun basin, with CC values ranging from 0.5 to 0.9, while lower CC values (0-0.5) were mainly found for Karkheh basin. ERA5-Land outperformed all other products and its estimates were well correlated with gauge observations ($CC > 0.7$) at the majority of stations. Corresponding bias-adjusted versions of CMORPH and TMPA products produced better results across the study area than their non-adjusted versions. However, PERSIANN-CDR showed no improvement on its real-time version. The poor performance of CMORPH-CRTV1.0 and PERSIANN might be due to inability of the PDF-matching-based bias-removal technique and cloud-top-based IR observations over complex terrains (Alijanian et al., 2017; Dinku et al., 2007). Based on this index, the worst results were produced by CHIRPSV2.0.

Among the unadjusted products, ERA5-Land significantly overestimated precipitation amount (bias > 1.35) in most regions, while other unadjusted products showed lower bias (Fig. S2). Dominant precipitation processes over complex topographies such as the Zagros mountains may have resulted in poor performance of ERA5-Land, which is consistent with findings by Fallah et al. (2020). The high bias rate for ERA5-Land may arise from its poor snowfall or precipitation detection, especially during wet months, while the lack of a proper snowfall removal process in ERA5-Land is reported to cause high overestimation for mountainous regions (Jiang et al., 2021; Orsolini et al., 2019). The spatial distribution of bias also showed that all products except ERA5-Land were susceptible to low bias rate for stations located in humid southeastern parts of Karun basin. In the arid southern regions of both basins, all products overestimated precipitation amount, with bias values ranging between 1.15 and 1.35. Thus the precipitation products tended to underestimate precipitation amount for wet regions and overestimate it for dry regions, which is consistent with previous results (Amjad et al., 2020; Chiaravalloti et al., 2018; De Leeuw et al., 2015; El Kenawy et al., 2015; Yuan et al., 2017).

Overall, the results showed that MERRA-2, PERSIANN-CDR, PGFV2.0, and CHIRPS had acceptable accuracy for a proportion of stations, with bias rate between 0.85 and 1.35. However, these products showed moderate to high overestimation for some stations, especially in mountainous regions in southeastern Karun basin. PERSIANN and CMORPH-RAWV1.0 showed the worst performance among all products, with strong underestimation (bias <0.45) mostly for stations located in the southeastern part of Karun basin.

The spatial distribution of variability ratio in daily time steps for all products is shown in Fig. S3. The bias-adjusted MERRA-2, CHIRPSV2.0, and TMPA-3B42V7.0 products were superior to other products in terms of variability ratio and had the highest number of stations with values close to the optimum (0.95-1.05). ERA5-Land, PERSIANN-CDR, CMORPH-RAWV1.0, JRA-55 and PERSIANN-CCS showed significant underestimation based on this index for most stations. Among all products, PERSIANN-CDR had the most stations with variability ratio <0.75 , indicating a high rate of underestimation for the study region. Interestingly, among all products with overestimation (variability ratio >1.15), the rate of overestimation was highest for stations located in southeast Karun basin and to some extent in northwest Karkheh basin. The results of variability ratio in daily time steps, along with all other statistical indicators, indicated that almost all products could not capture accurately the spatial variability in precipitation across both basins. Therefore, effective preprocessing methods must be considered prior to utilizing these products for complex terrain.

The performance of different precipitation products over the study area, in terms of the contingency table of POD, FAR, and HSS, is compared and evaluated in Figures 8-10. ERA5-Land greatly outperformed all other products, with the highest POD value (>0.7). However, this might come at the cost of overestimating precipitation events, as ERA5-Land also displayed the

greatest bias rate (see Figs. 4-6) and highest FAR values for the study area (Fig. 9). This is in line with previous findings (Amjad et al., 2020; De Leeuw et al., 2015; Gampe and Ludwig, 2017; Hénin et al., 2018) for both the ERA5 and ERA-interim products. PERSIANN-CCS, PERSIANN-CDR, JRA-55, and CMORPH-BLDV1.0 showed acceptable accuracy and performed better than the other products in terms of POD index (Fig. 8). Interestingly and in contrast to the results for daily KGE index, calibration of PERSIANN-CDR and CMORPH-BLDV1.0 using gauge information significantly improved their rainfall detection capability. However, this was not the case for CMORPH-CRTV1.0 and TMPA-3B42V7.0, the adjusted versions of CMORPH-RAWV1.0 and TMPA-3B42RTV7.0, respectively. Overall, CHIRPSV2.0, CMORPH-RAWV1.0, and PERSIANN had the worst results of all products, based on POD index (Fig. 8).

Although the precipitation products performed relatively well in detecting rainy days, the FAR values were slightly high for all products across both basins (Fig. 9), showing lower ability of all products in detecting “no rainy” events. This was particularly the case for ERA5-Land, as explained before considering its high POD value. Conversely, CMORPH-RAWV1.0 which provided the lowest POD index values in Fig. 8, performed better than all other products in terms of FAR index, explaining the high underestimation of observed precipitation by CMORPH-RAW1.0 across both basins (Fig. 9). Interestingly, the spatial distribution of FAR index indicated that bias-adjusted products reduced the accuracy of their unadjusted versions, especially for PERSIANN-CDR. This might be because improving either FAR or POD usually leads to the deterioration of the other, as there is a trade-off between the ability of a model in detecting rainy days (high POD) and falsely reporting them (high FAR) (Ghajarnia et al., 2016). The FAR values showed no particular spatial pattern across the study area (Fig. 9).

506 Fig. 10 demonstrates the ability of products in correct detection of rainfall events based on the
507 HSS index. CMORPH-BLDV1.0 and MSWEPV2.0 had the highest accuracy among all products
508 in terms of HSS, with values >0.6 across the study area. In addition, MERRA-2 and ERA5-Land
509 showed acceptable performance for both basins, but none of the products performed well for the
510 northern mountainous region in Karun basin (HSS values around 0.3). CHIRPSV2.0, CMORPH-
511 RAWV1.0, TMPA-3BRTV7.0, and PERSIANN showed the worst performance across both basins
512 (CHIRPSV2.0 had the worst results of all products). Comparing the spatial distribution of HSS for
513 unadjusted and bias-adjusted versions of the products (Fig. 10), the results indicated enhanced
514 performance of the adjusted versions, particularly in the PERSIANN and TMPA families, where
515 the bias-adjusted versions showed higher HSS in southern areas of the Karun basin.

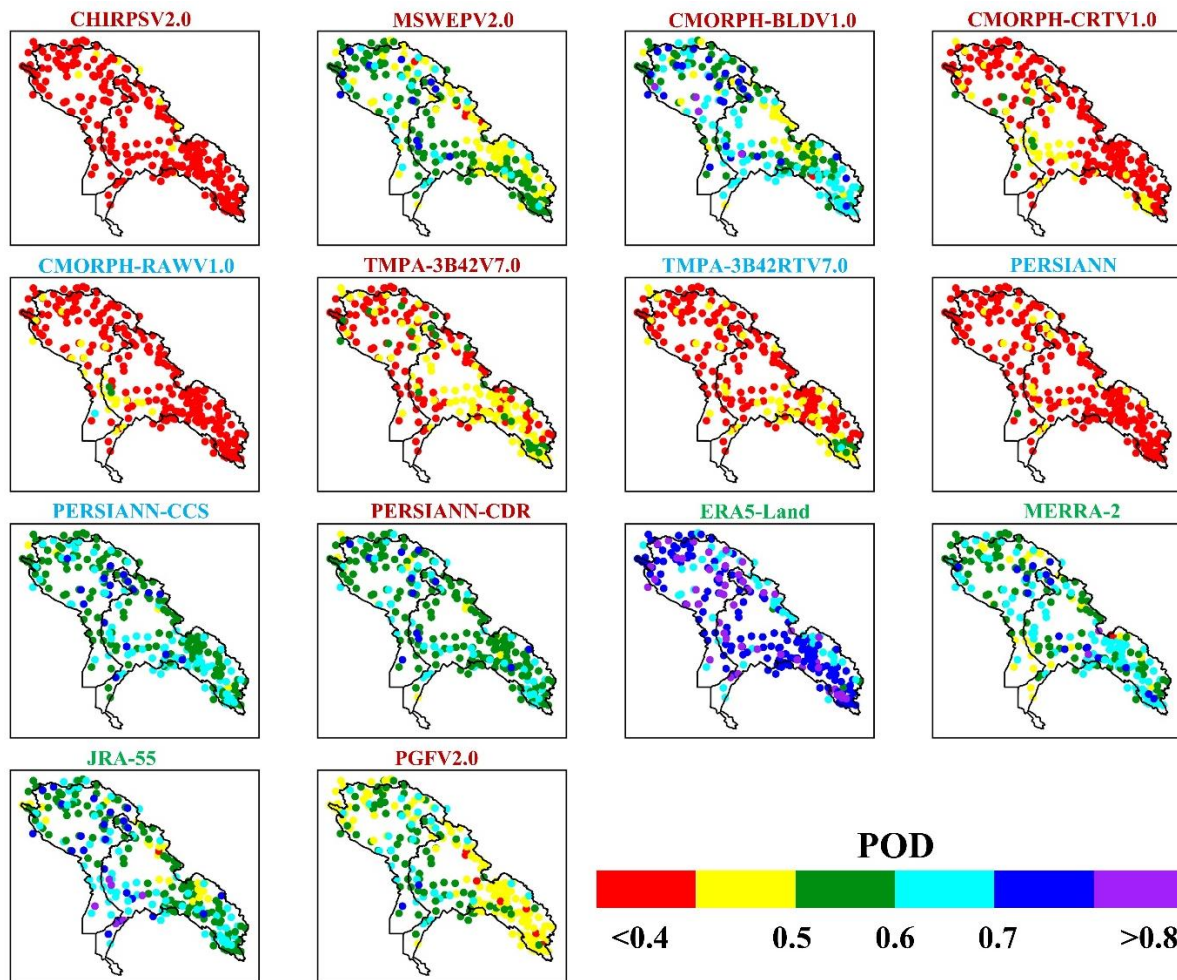


Fig. 8. Spatial distribution of Probability of Detection (POD) index for global precipitation products versus gauge observations. Blue, red, and green indicates satellite-based, multi-source, and reanalysis precipitation products, respectively.

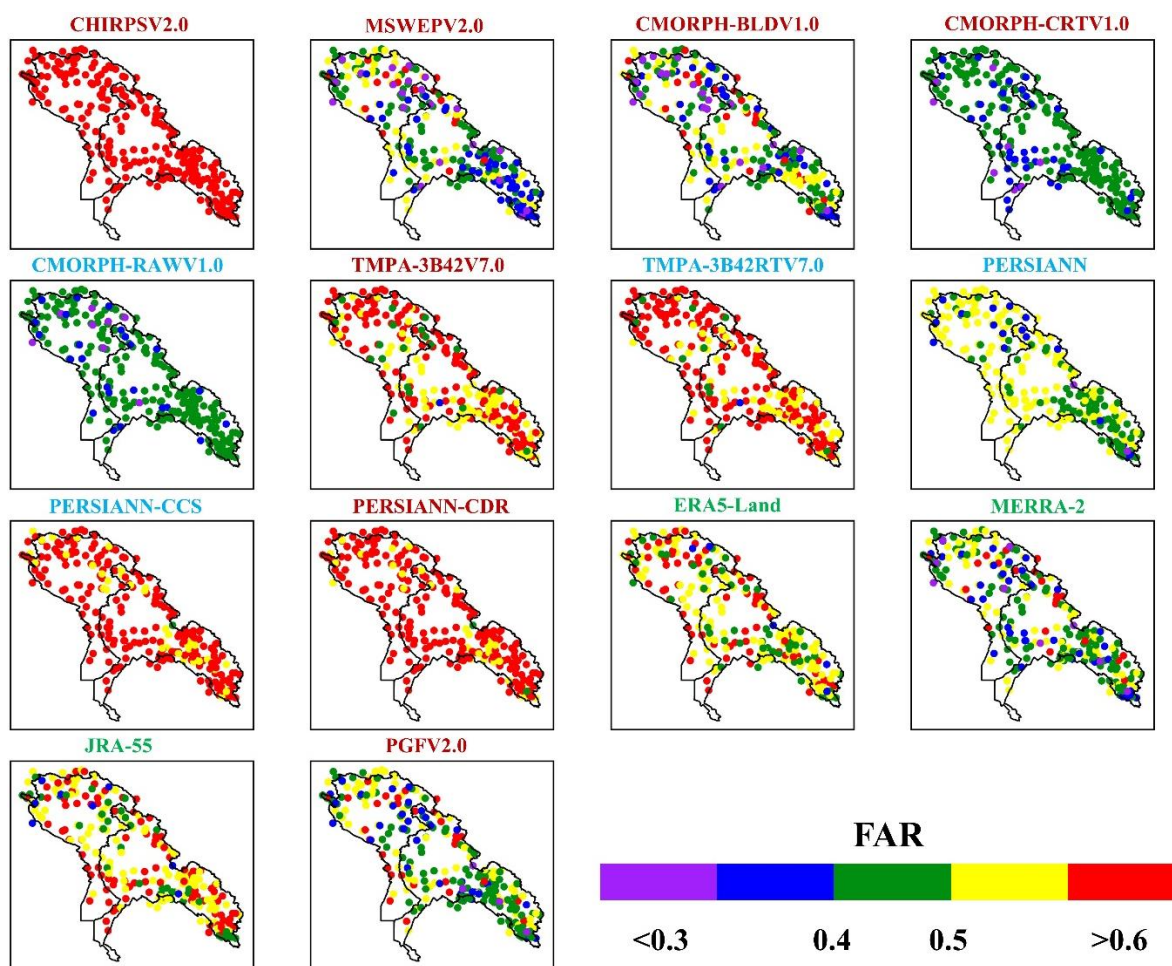


Fig. 9. Spatial distribution of False Alarm Ratio (FAR) index for global precipitation products versus gauge observations. Blue, red, and green indicates satellite-based, multi-source, and reanalysis precipitation products, respectively.

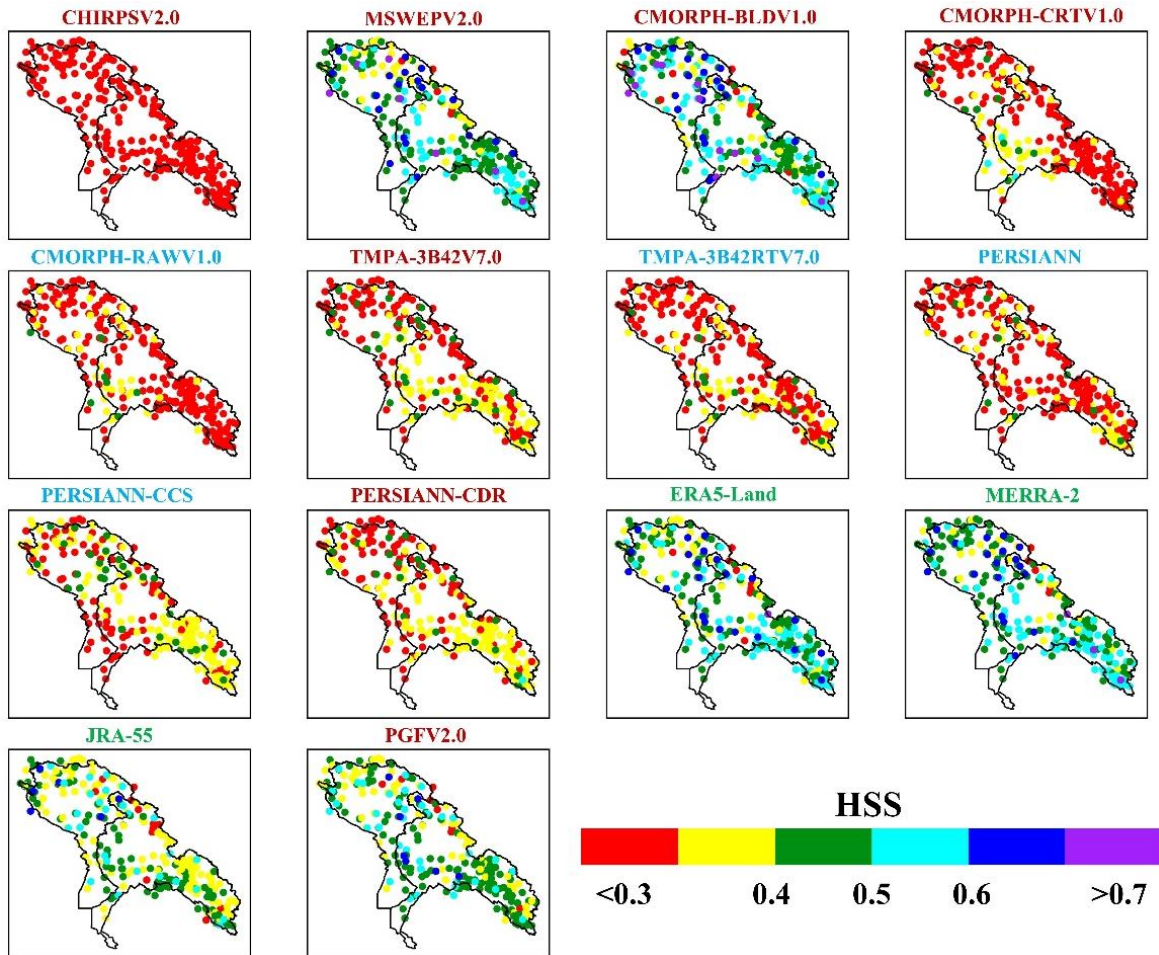


Fig. 10. Spatial distribution of Heidke Skill Score (HSS) for global precipitation products versus gauge observations step. Blue, red, and green indicates satellite-based, multi-source, and reanalysis precipitation products, respectively.

3.3. Statistical analysis of global precipitation products at monthly time steps

To examine the performance of the global precipitation products more thoroughly at monthly scale, which is appropriate temporal resolution for water resources and climate change studies, the evaluations were repeated based on monthly time series. Compared with daily results (see Fig. 6), monthly KGE scores varied over a wider range at monthly time steps and reached higher values (Fig. 11). TMPA-3B42V7.0, PERSIANN-CDR, MERRA-2, and PGFV2.0 outperformed other products in terms of monthly KGE score, with average KGE values >0.5 . The bias-adjusted

535 products (TMPA-3B42V7.0, PERSIANN-CDR, CMORPH-BLDV1.0, and CMORPH-CRTV1.0)
536 showed better monthly KGE scores than their unadjusted versions. Surprisingly, TMPA-
537 3B42RTV7.0, JRA-55, and PERSIANN-CCS, which are basically unadjusted products, performed
538 even better than some bias-adjusted products such as MSWEPV2.0, CMORPH-BLDV1.0,
539 CHIRPSV2.0, and CMORPH-CRTV1.0. Comparing the results of PERSIANN-CDR at monthly
540 and daily time steps revealed that the significant improvement in its precipitation estimations at
541 monthly time steps might be related to the calibration of PERSIANN-CDR with monthly GPCP
542 data (Ashouri et al., 2015). The results also indicated higher CC values in comparison with daily
543 values, and for the majority of the studied products (Fig. S4). MSWEPV2.0 and ERA5-Land also
544 had very high monthly CC, but their KGE values were low due to their high under- and
545 overestimation, respectively (low and high bias index). The high CC value obtained for
546 MSWEPV2.0 might be related to its algorithm, in which observational data receive higher weights
547 based on their CC in the merging scheme (Beck et al., 2019b). All products were relatively
548 successful in representing the monthly variation in observed precipitation, as the variability indices
549 mostly ranged around the optimum value (unity).

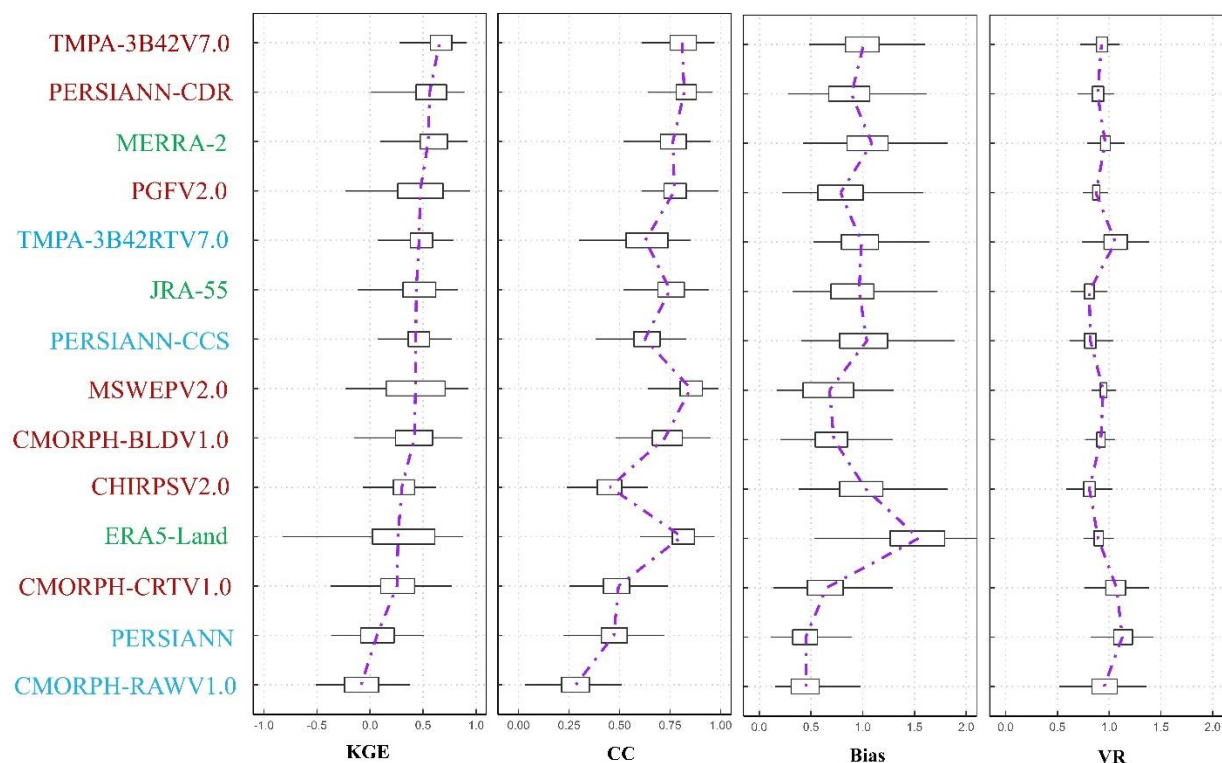


Fig. 11. Reliability of the precipitation products at regional scale in monthly time steps 2003-2012. The products are arranged from most (top) to least (bottom) efficient in terms of average Kling-Gupta Efficiency (KGE).

Figure 12 shows the spatial distribution of KGE score for the different global precipitation products. The overall spatial pattern of KGE score suggested that almost all products (except CMORPH-RAWV1.0, CMORPH-CRTV1.0, and PERSIANN) performed well in Karkheh basin, with improved performance of the bias-adjusted versions. However, in Karun basin with its more diverse topographical conditions and higher mountains, MERRA-2, PERSIANN-CDR, and TPMA-3B42V7.0 performed moderately well, while other products showed poor performance. The results also indicated that reanalysis products were significantly different from each other, with MERRA-2 having high accuracy across both basins, while ERA5-Land and JRA-55 showed poor to moderate accuracy. The bias-adjusted products of MSWEPV2.0, CMORPH-CRTV1.0,

and PGFV2.0 showed poor performance across mountainous regions, indicating unsuccessful bias adjustments in the study area. The main reasons for this might be inherent limitations of the calibration procedure and lack of a gauge network in remote highlands (Dahri et al., 2021).

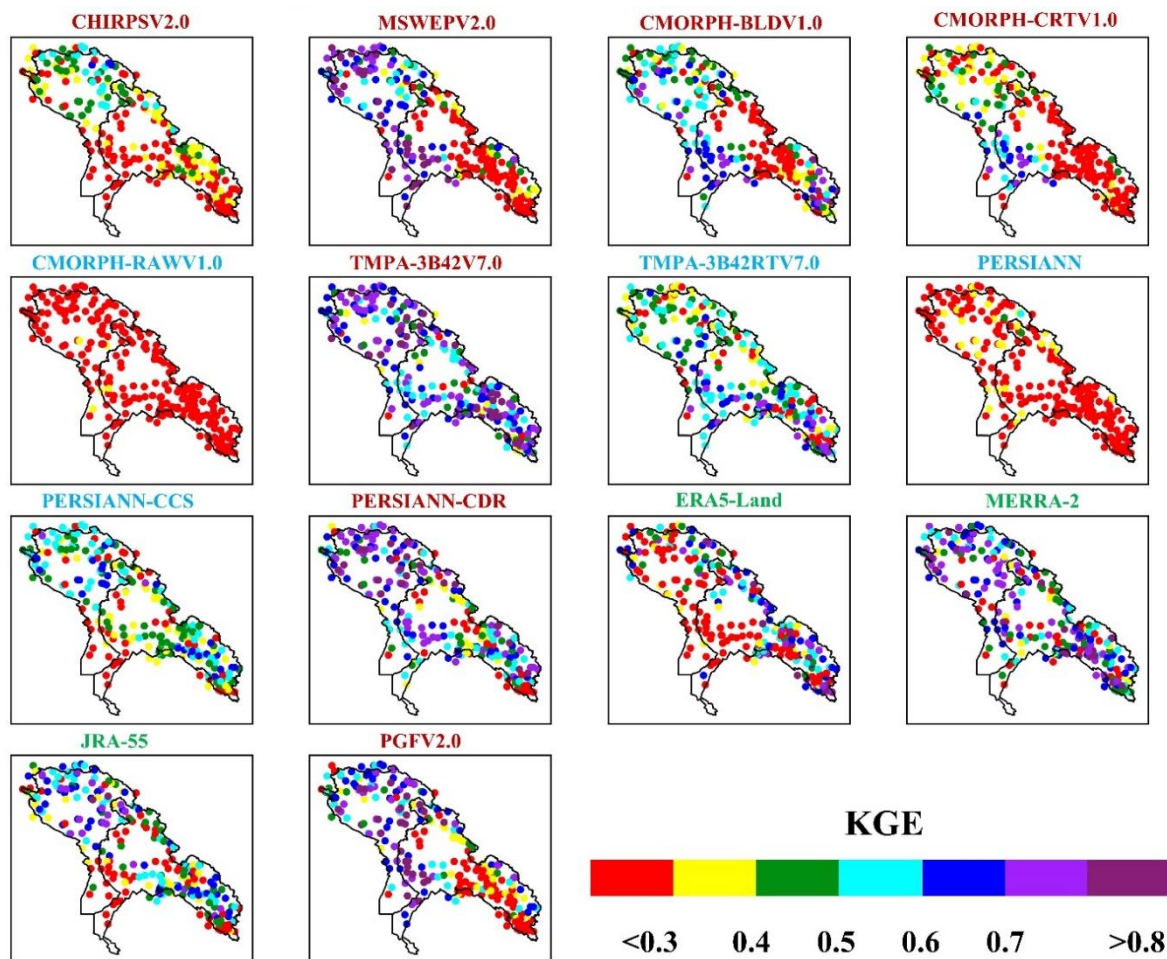


Fig. 12. Spatial distribution of Kling-Gupta Efficiency (KGE) index for global precipitation products versus gauge observations in monthly time steps. Blue, red, and green indicates satellite-based, multi-source, and reanalysis precipitation products, respectively.

The spatial distributions of CC and variability index are shown in Figs S4 and S5 in Supplementary Information. Due to the similarity of bias at monthly and daily time steps, monthly biases are not reported again in this section. All products except CMORPH-RAWV1.0, CMORPH-CRTV1.0, PERSIANN, and CHIRPSV2.0 were well correlated with gauge records ($CC > 0.7$), and showed

their best performance for stations located in the west and southeast of the study area (Fig. S4). Compared with daily time steps (Fig. S1), bias-adjusted precipitation products provided higher accuracy and were more reliable across both basins at monthly time steps. However, the differences between bias-adjusted and unadjusted versions were more negligible at daily compared with monthly time steps, which means more efficient adjustments in monthly outputs of the models. This is in line with previous findings (Alijanian et al., 2017) on the performance of PERSIANN, PERSIANN-CDR, TMPA-3B42V7.0, and MSWEP at different temporal scales in Iran indicating that the CC value increases significantly at monthly time steps compared with daily time steps. Fallah et al. (2020) found that based on monthly CC index, ERA5 performed well, whereas JRA-55 and MSWEPV2.0 showed relatively poor performance in Karun basin, which was contradictory to our findings. This might be due to the lower gauge density of the reference dataset in Fallah et al. (2020) or the difference between the study periods in the evaluations (2000-2015 in Fallah et al. (2020), as opposed to 2003-2012 in this study).

Figure S5 shows the spatial distribution of variability ratio in global precipitation products over the study area. The bias-adjusted products MERRA-2, MSWEPV2.0, CMORPH-BLDV1.0, and TMPA-3B42V7.0 were able to better capture the precipitation variability across the two basins (variability ratio between 0.9 and 1.05 in most regions), indicating that these products could be used to predict monthly precipitation variability with higher confidence level. However, the CHIRPSV2.0, JRA-55, and PERSIANN-CDR products largely underestimated precipitation variability, particularly in southwestern parts of the study area (variability ratio below 0.85). In addition, some products showed great overestimation in the north of Karkheh basin (PERSIANN, CMORPH-CRTV1.0, and CMORPH-RAWV1.0) and in the mountainous southeastern part of Karun basin (PERSIANN, CMORPH-CRTV1.0, and TMPA-3B42RTV7.0). Overall, considering

the variability ratio of the bias-adjusted versions of PERSIANN, TRMM, and CMORPH (but not CMORPH-CRTV1.0), it is evident that the use of gauge records converted the overestimated outputs of these products to optimum or underestimated values.

3.4. Model rankings and summary of evaluations

A performance diagram (Roebber, 2009) was created to summarize the results. This diagram uses the categorical indicators POD, SR (Success Ratio), CSI (as labeled solid contours) and bias (as dashed lines with labels on the outward extension of the line) and summarizes model performance based on contingency table indices, with the best values in the top right and the worst in the bottom left corner. To evaluate the performance of the 14 precipitation products for different precipitation levels, precipitation intensity was divided into four categories: 0-5, 5-10, 10-20, and ≥ 20 mm/day, indicating light, moderate, heavy, and extreme rainfall, respectively.

The performance diagram for all products (Fig. 13) indicated that MERRA-2, CMORPH-BLDV1.0, MSWEPV2.0, PGFV2.0, JRA-55, and ERA5-Land outperformed other products in correctly capturing precipitation occurrences, followed by PERSIANN-CDR. The results also indicated that bias-adjusted versions of PERSIANN (PERSIANN-CDR) and CMORPH (CMORPH-BLDV1.0 and CMORPH-CRTV1.0) performed better than their unadjusted versions (Fig. 13). In the TMPA family, incorporation of gauge information did not improve estimation of precipitation occurrence by TMPA-3B42V7.0. Surprisingly, all products had a near-perfect score in detecting light rainfall events (0-5 mm/day). However, the performance of all products in detecting moderate (5-10 mm/day) and heavy (10-20 mm/day) precipitation events deteriorated. Points were closer to the no skill area for the moderate class and scattered in the plot (with better performance of ERA5-Land) for the heavy precipitation class. ERA5-Land, followed by MERRA-2, outperformed other products in detecting extreme precipitation events (Fig. 13). For this

620 precipitation category JRA-55, PERSIANN-CDR, CMORPH-BLDV1.0, and MSWEPV2.0
621 performed similarly, with SR <0.5, POD <0.2, CSI <0.2, and bias varying from 0.3 to 0.5.
622 CMORPH-RAWV1.0, and CHIRPSV2.0 were the worst products at capturing heavy and extreme
623 precipitation events. TMPA-3B42RTV7.0 showed similar performance to TMPA-3B42V7.0,
624 while other bias-adjusted products (CMORPH-BLDV1.0, CMORPH-CRTV1.0, and PERSIANN-
625 CDR) outperformed their unadjusted versions in the heavy precipitation class. Overall, the
626 performance diagram indicated that ERA5-Land and MERRA-2 performed better than the other
627 products, particularly in reproducing rainfall events above 20 mm/day (Fig. 13). However, all
628 products seemed to perform well in capturing rainfall events in the light intensity class. Previously,
629 Nashwan et al. (2020) found better performance for Global Satellite Mapping of Precipitation
630 (GSMaP) (Ushio et al., 2009) and African Rainfall Climatology (ARC) (Novella and Thiaw, 2013)
631 for the 0-5 mm/day precipitation class in Egypt.

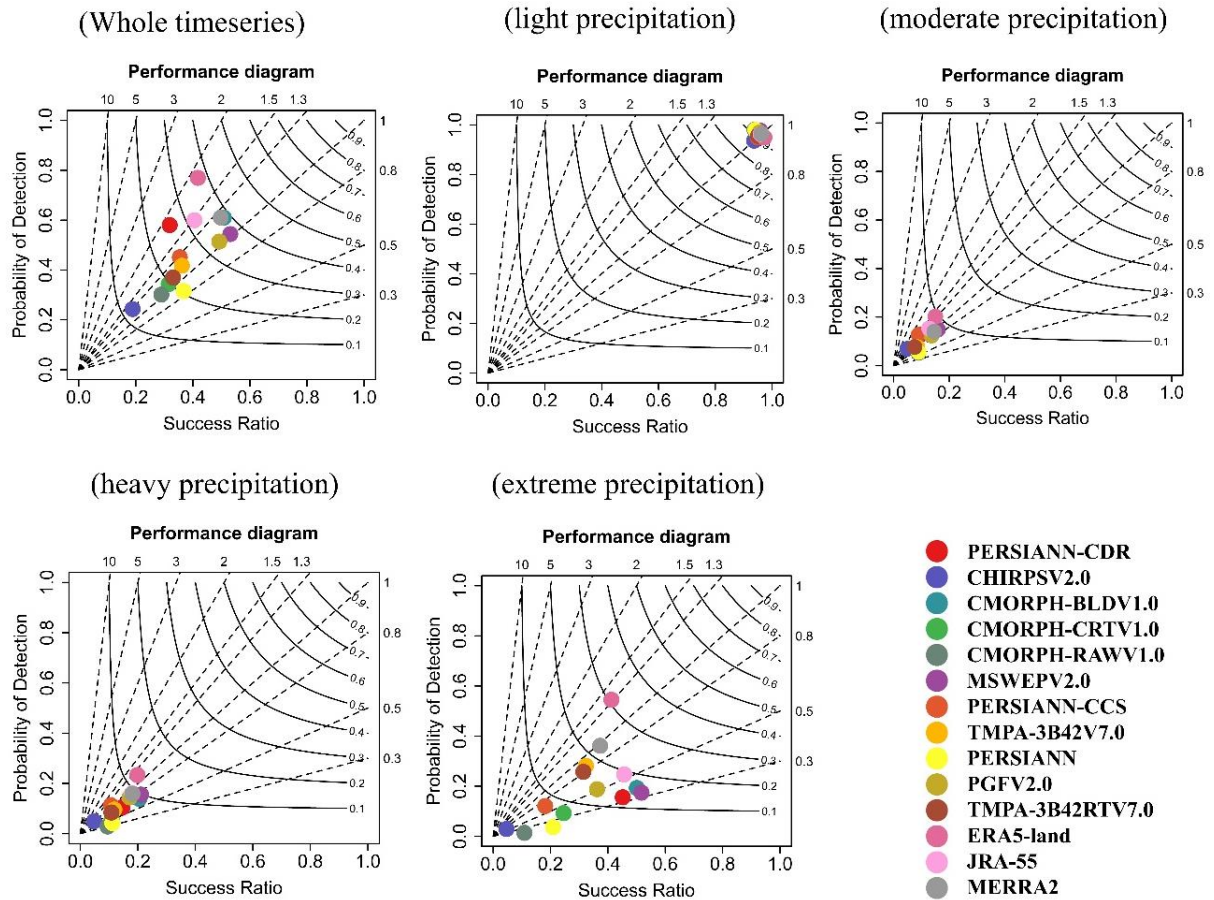


Fig. 13. Performance diagram summarizing the results of contingency table indices for global precipitation products at different precipitation intensity and the whole time series. The light, moderate, heavy, and extreme class corresponds to 0-5, 5-10, 10-20, and ≥ 20 mm/day, respectively. Points closer to the top right corner indicate better ability of models in correctly detecting precipitation occurrence.

The overall ranking of different precipitation products in term of average monthly and daily KGE scores (Fig. 14) showed that the performance of products at monthly time scale was around twice as good as at daily time scale. This might have been influenced by merging the monthly observational datasets in some products, e.g., PERSIANN-CDR. PERSIANN-CDR was the worst performing product at daily time scale, with even worst performance than PERSIANN (Fig. 14a). However, its performance improved considerably at monthly time scale, when PERSIANN-CDR was the second best product (Fig. 14b). Conversely, the performance of CMORPH-BLDV1.0

deteriorated from daily to monthly time scale (Fig. 14). Based on the average KGE index, TMPA-3B42V7.0, MERRA-2, and PGFV2.0 were the three best-performing products in estimation of precipitation rates, both at daily and monthly time scales. CMORPH-BLDV1.0 and PERSIANN-CDR were also among the best products, but only at daily and monthly scale, respectively.

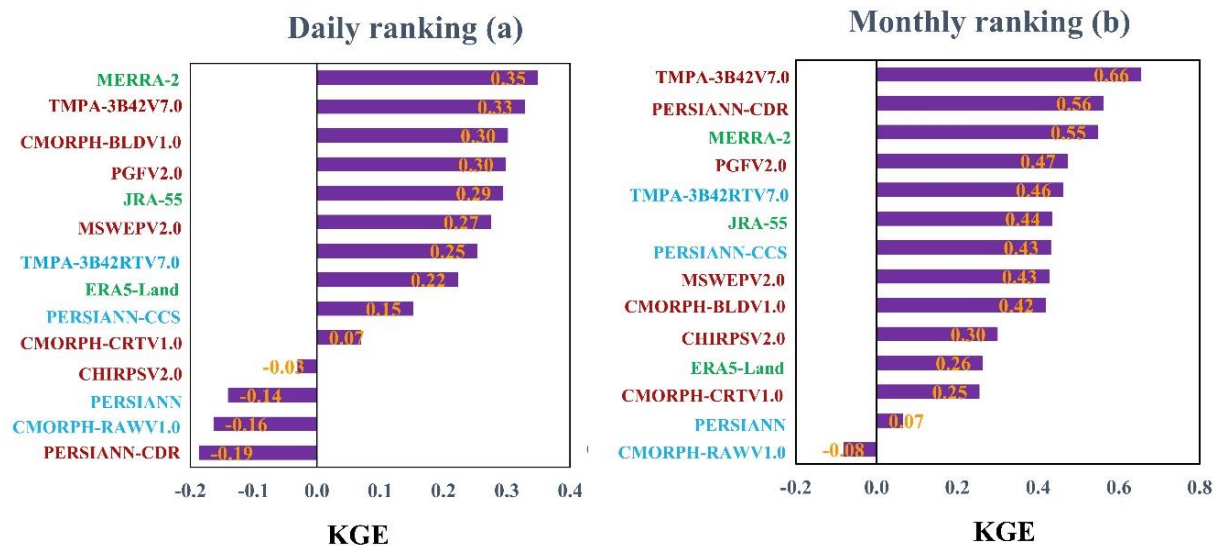


Fig. 14. Ranking of global precipitation products based on (a) daily and (b) monthly Kling-Gupta Efficiency (KGE) index.

4. Conclusions

The performance of 14 high-resolution precipitation products (CMORPH-RAWV1.0, CMORPH-BLDV1.0, CMORPH-CRTV1.0, PERSIANN, PERSIANN-CDR, PERSIANN-CDR, MSWEPV2.0, PGFV2.0, JRA-55, ERA5-Land, MERRA-2, CHIRPSV2.0, TMPA-3B42RTV7.0, TMPA-3B42V7.0) in estimating daily and monthly precipitation in Karun and Karkheh basins, Iran, 2003-2012 was evaluated and compared against reference observations from 254 local gauges across both basins. Different statistical, categorical, and visualization methods were used to scrutinize different aspects of the performance of the global precipitation products. The conclusions obtained were as follows:

1. Comparison of MAP maps based on observational data and global precipitation products revealed that TMPA-3B42 (both versions), ERA5-LAND, and MERRA-2 provided better annual estimates for the whole study area.
2. For annual time series of precipitation averaged over the whole study area, all products except CHIRPSV2.0 achieved similar performance in capturing changes in annual observed precipitation after 2004. At monthly time steps, TMPA-3B42V7.0 outperformed all other products, with estimates closest to the reference observations. ERA5-Land overestimated annual precipitation, while all other products were either close to or underestimated the reference dataset.
3. Statistical evaluation revealed poor accuracy of all products at daily time scale, but all bias-adjusted products except PERSIANN-CDR outperformed their unadjusted version. ERA5-Land was not among the best-performing products at daily time scale. Its high CC value denoted good correlation with observed precipitation over the study area, but its high bias rate and low variability ratio led to relatively low KGE score.
4. Three categorical metrics were employed (POD, FAR, HSS). Based on POD, ERA5-Land, PERSIANN-CCS, PERSIANN-CDR, JRA-55, and CMORPH-BLDV1.0 were the best-performing products. In addition, all bias-adjusted products outperformed their unadjusted versions based on POD. Based on FAR, correction lowered the performance of uncorrected versions. Based on the overall HSS index, CMORPH-BLD V1.0, MSWEPV2.0, MERRA-2, and ERA5-Land outperformed other products across the study area. None of the products performed well in mountainous areas in Karun basin.
5. Statistical indices indicated considerable improvement in the performance of all products when applied to monthly results, almost twice as good as for daily time steps. In term of monthly KGE, TMPA-3B42V7.0, PERSIANN-CDR, and MERRA-2 were the best-performing products, with average KGE >0.5. Due to the complex precipitation pattern over highland areas, all products except TMPA-3B42V7.0, PERSIANN-CDR, and MERRA-2 showed poor accuracy in these

regions based on the KGE index. Overall, based on all indices at monthly time scale, bias-adjusted products outperformed their unadjusted versions.

6. A performance diagram showed good reliability of all products for the light rainfall category (0-5 mm/day), but poor accuracy for moderate to heavy precipitation classes. ERA5-Land outperformed other products in detecting rainfall occurrences above 10 mm/day, with ERA5-Land joining it for the extreme precipitation class (>20 mm/day). Ranking the products in terms of accurate estimation of precipitation rates based on average KGE index showed that TMPA-3B42V7.0 and MERRA-2 were the two most reliable products at both daily and monthly time scale across Karun and Karkheh basins in southwest Iran.

These findings provide better insights on the performance of different global precipitation products for two crucial and threatened basins in Iran and can support other hydrological and water resources studies in the region. The differences found between products in estimating precipitation at daily or monthly time scale show the importance of evaluations of this type, which can allow other researchers to choose their preferred products based on their specific needs and preferences.

Acknowledgments

This study arose from a project funded by Formas, 2017-00,608.

Author Contribution

Author contributions were as follows: A. R., A. B., and A. S. equally contributed to data curation, methodology, visualization, result analysis and were mainly responsible for writing the paper; Z. K. contributed to the result analysis, writing, reviewing, and editing; A. M. B. contributed to the result analysis, writing, reviewing, and editing; N.G. lead the study, contributed to the methodology, result analysis, writing, reviewing, and editing.

References

- Ababaei, B., Etedali, H.R., 2021. Investigating Spatiotemporal Variations of Precipitation across Iran over 1957-2016 using the CRU Gridded Dataset. *Quranic Knowl. Res.* 21, 103–117.
- Adler, R.F., Huffman, G.J., Chang, A., Ferraro, R., Xie, P.-P., Janowiak, J., Rudolf, B., Schneider, U., Curtis, S., Bolvin, D., others, 2003. The version-2 global precipitation climatology project (GPCP) monthly precipitation analysis (1979--present). *J. Hydrometeorol.* 4, 1147–1167.
- Afkhami, M., Shariat, M., Jaafarzadeh, N., Ghadiri, H., Nabizadeh, R., 2007. Regional water quality management for the Karun–Dez River basin, Iran. *Water Environ. J.* 21, 192–199.
- Ahmad, M.-D., Giordano, M., 2010. The Karkheh River basin: the food basket of Iran under pressure. *Water Int.* 35, 522–544.
- Alijanian, M., Rakhshandehroo, G.R., Mishra, A.K., Dehghani, M., 2017. Evaluation of satellite rainfall climatology using CMORPH, PERSIANN- CDR, PERSIANN, TRMM, MSWEP over Iran. *Int. J. Climatol.* 37, 4896–4914.
- Amjad, M., Yilmaz, M.T., Yucel, I., Yilmaz, K.K., 2020. Performance evaluation of satellite- and model-based precipitation products over varying climate and complex topography. *J. Hydrol.* 584, 124707. <https://doi.org/https://doi.org/10.1016/j.jhydrol.2020.124707>
- Asante, K.O., Macuacua, R.D., Artan, G.A., Lietzow, R.W., Verdin, J.P., 2007. Developing a flood monitoring system from remotely sensed data for the Limpopo basin. *IEEE Trans. Geosci. Remote Sens.* 45, 1709–1714.
- Ashouri, H., Hsu, K.-L., Sorooshian, S., Braithwaite, D.K., Knapp, K.R., Cecil, L.D., Nelson, B.R., Prat, O.P., 2015. PERSIANN-CDR: Daily precipitation climate data record from multisatellite observations for hydrological and climate studies. *Bull. Am. Meteorol. Soc.* 96, 69–83.
- Awange, J.L., Hu, K.X., Khaki, M., 2019. The newly merged satellite remotely sensed, gauge and reanalysis-based Multi-Source Weighted-Ensemble Precipitation: Evaluation over Australia and Africa (1981–2016). *Sci. Total Environ.* 670, 448–465.
- Azizi, G., Safarrad, T., Mohammadi, H., Faraji Sabokbar, H., 2016. Evaluation and comparison of reanalysis precipitation data in Iran. *Phys. Geogr. Res. Q.* 48, 33–49.
- Azizian, A., Ramezani etedali, hadi, 2019. Assessing the Accuracy of European Center for Medium Range Weather Forecasts (ECMWF) Reanalysis Datasets for Estimation of Daily and Monthly Precipitation. *Iran. J. Soil Water Res.* 50, 777–791. <https://doi.org/10.22059/ijswr.2018.261613.667962>
- Azizian, A., Ramezani Etedali, H., 2019. Spatiotemporal Assessment of Reanalysis and Remotely-Sensed Precipitation Datasets. *Iran-Water Resour. Res.* 15, 163–177.
- Beck, H.E., Pan, M., Roy, T., Weedon, G.P., Pappenberger, F., Van Dijk, A.I.J.M., Huffman, G.J., Adler, R.F., Wood, E.F., 2019a. Daily evaluation of 26 precipitation datasets using Stage-IV gauge-radar data for the CONUS. *Hydrol. Earth Syst. Sci.* 23, 207–224. <https://doi.org/10.5194/hess-23-207-2019>
- Beck, H.E., Wood, E.F., Pan, M., Fisher, C.K., Miralles, D.G., Van Dijk, A.I.J.M., McVicar, T.R., Adler, R.F., 2019b. MSWep v2 Global 3-hourly 0.1° precipitation: Methodology and quantitative assessment. *Bull. Am. Meteorol. Soc.* 100, 473–500. <https://doi.org/10.1175/BAMS-D-17-0138.1>
- Brunetti, M., Maugeri, M., Monti, F., Nanni, T., 2006. Temperature and precipitation variability in Italy

747 in the last two centuries from homogenised instrumental time series. *Int. J. Climatol.* A J. R.
748 *Meteorol. Soc.* 26, 345–381.

749 Carrera-Hernandez, J.J., Gaskin, S.J., 2007. Spatio temporal analysis of daily precipitation and
750 temperature in the Basin of Mexico. *J. Hydrol.* 336, 231–249.

751 Chiaravallotti, F., Brocca, L., Procopio, A., Massari, C., Gabriele, S., 2018. Assessment of GPM and
752 SM2RAIN-ASCAT rainfall products over complex terrain in southern Italy. *Atmos. Res.* 206, 64–
753 74.

754 Choubin, B., Solaimani, K., Rezanezhad, F., Roshan, M.H., Malekian, A., Shamshirband, S., 2019.
755 Streamflow regionalization using a similarity approach in ungauged basins: Application of the geo-
756 environmental signatures in the Karkheh River Basin, Iran. *Catena* 182, 104128.

757 Dahri, Z.H., Ludwig, F., Moors, E., Ahmad, S., Ahmad, B., Shoaib, M., Ali, I., Iqbal, M.S., Pomee, M.S.,
758 Mangrio, A.G., 2021. Spatio- temporal evaluation of gridded precipitation products for the high-
759 altitude Indus basin. *Int. J. Climatol.*

760 Darand, M., Amanollahi, J., Zandkarimi, S., 2017. Evaluation of the performance of TRMM Multi-
761 satellite Precipitation Analysis (TMPA) estimation over Iran. *Atmos. Res.* 190, 121–127.

762 Darand, M., Khandu, K., 2020. Statistical evaluation of gridded precipitation datasets using rain gauge
763 observations over Iran. *J. Arid Environ.* 178, 104172.
764 <https://doi.org/10.1016/j.jaridenv.2020.104172>

765 De Leeuw, J., Methven, J., Blackburn, M., 2015. Evaluation of ERA- Interim reanalysis precipitation
766 products using England and Wales observations. *Q. J. R. Meteorol. Soc.* 141, 798–806.

767 Dee, D.P., Uppala, S.M., Simmons, A., Berrisford, P., Poli, P., Kobayashi, S., Andrae, U., Balmaseda,
768 M., Balsamo, G., Bauer, d P., Others, 2011. The ERA-Interim reanalysis: Configuration and
769 performance of the data assimilation system. *Q. J. R. Meteorol. Soc.* 137, 553–597.

770 Derin, Y., Anagnostou, E., Berne, A., Borga, M., Boudevillain, B., Buytaert, W., Chang, C.-H., Delrieu,
771 G., Hong, Y., Hsu, Y.C., Lavado-Casimiro, W., Manz, B., Moges, S., Nikolopoulos, E.I., Sahl, D.,
772 Salerno, F., Rodríguez-Sánchez, J.-P., Vergara, H.J., Yilmaz, K.K., 2016. Multiregional Satellite
773 Precipitation Products Evaluation over Complex Terrain. *J. Hydrometeorol.* 17, 1817–1836.
774 <https://doi.org/10.1175/JHM-D-15-0197.1>

775 Dinku, T., Ceccato, P., Grover- Kopeck, E., Lemma, M., Connor, S.J., Ropelewski, C.F., 2007. Validation
776 of satellite rainfall products over East Africa’s complex topography. *Int. J. Remote Sens.* 28, 1503–
777 1526.

778 Duan, Z., Liu, J., Tuo, Y., Chiogna, G., Disse, M., 2016. Evaluation of eight high spatial resolution
779 gridded precipitation products in Adige Basin (Italy) at multiple temporal and spatial scales. *Sci.*
780 *Total Environ.* 573, 1536–1553.

781 El Kenawy, A.M., Lopez-Moreno, J.I., McCabe, M.F., Vicente-Serrano, S.M., 2015. Evaluation of the
782 TMPA-3B42 precipitation product using a high-density rain gauge network over complex terrain in
783 northeastern Iberia. *Glob. Planet. Change* 133, 188–200.

784 Fallah, A., Rakhshandehroo, G.R., Berg, P., Sungmin, O., Orth, R., 2020. Evaluation of precipitation
785 datasets against local observations in southwestern Iran. *Int. J. Climatol.* 40, 4102–4116.
786 <https://doi.org/10.1002/joc.6445>

787 Funk, C., Peterson, P., Landsfeld, M., Pedreros, D., Verdin, J., Shukla, S., Husak, G., Rowland, J.,
788 Harrison, L., Hoell, A., 2015. The climate hazards infrared precipitation with stations—a new

789 environmental record for monitoring extremes. *Sci. data* 2, 1–21.

790 Funk, C.C., Peterson, P.J., Landsfeld, M.F., Pedreros, D.H., Verdin, J.P., Rowland, J.D., Romero, B.E.,
791 Husak, G.J., Michaelsen, J.C., Verdin, A.P., 2014. A quasi-global precipitation time series for
792 drought monitoring. *US Geol. Surv. data Ser.* 832, 1–12.

793 Gampe, D., Ludwig, R., 2017. Evaluation of gridded precipitation data products for hydrological
794 applications in complex topography. *Hydrology* 4, 53.

795 Ghajarnia, N., Abdolmajid, L., Daneshkar Arasteh, P., 2014. Verifying precipitation data of TAMAB and
796 meteorology institute in Urmia basin. *J. Soil Water Resour. Conserv.* 4, 91–109.

797 Ghajarnia, N., Arasteh, P.D., Araghinejad, S., Liaghat, M.A., 2016. A hybrid Bayesian-SVD based
798 method to detect false alarms in PERSIANN precipitation estimation product using related physical
799 parameters. *J. Hydrol.* 538, 640–650.

800 Ghajarnia, N., Kalantari, Z., Destouni, G., 2020. Data-driven worldwide quantification of large-scale
801 hydroclimatic co-variation patterns and comparison with reanalysis and Earth System 2 modeling 3.

802 Ghajarnia, N., Liaghat, A., Daneshkar Arasteh, P., 2015. Comparison and evaluation of high resolution
803 precipitation estimation products in Urmia Basin-Iran. *Atmos. Res.* 158–159, 50–65.
804 <https://doi.org/10.1016/j.atmosres.2015.02.010>

805 Gupta, H. V., Kling, H., Yilmaz, K.K., Martinez, G.F., 2009. Decomposition of the mean squared error
806 and NSE performance criteria: Implications for improving hydrological modelling. *J. Hydrol.* 377,
807 80–91.

808 Harris, I., Jones, P.D., Osborn, T.J., Lister, D.H., 2014. Updated high- resolution grids of monthly
809 climatic observations—the CRU TS3. 10 Dataset. *Int. J. Climatol.* 34, 623–642.

810 Hénin, R., Liberato, M.L.R., Ramos, A.M., Gouveia, C.M., 2018. Assessing the use of satellite-based
811 estimates and high-resolution precipitation datasets for the study of extreme precipitation events
812 over the Iberian Peninsula. *Water* 10, 1688.

813 Hersbach, H., Bell, B., Berrisford, P., Hirahara, S., Horányi, A., Muñoz-Sabater, J., Nicolas, J., Peubey,
814 C., Radu, R., Schepers, D., Simmons, A., Soci, C., Abdalla, S., Abellan, X., Balsamo, G., Bechtold,
815 P., Biavati, G., Bidlot, J., Bonavita, M., De Chiara, G., Dahlgren, P., Dee, D., Diamantakis, M.,
816 Dragani, R., Flemming, J., Forbes, R., Fuentes, M., Geer, A., Haimberger, L., Healy, S., Hogan,
817 R.J., Hólm, E., Janisková, M., Keeley, S., Laloyaux, P., Lopez, P., Lupu, C., Radnoti, G., de
818 Rosnay, P., Rozum, I., Vamborg, F., Villaume, S., Thépaut, J.N., 2020. The ERA5 global reanalysis.
819 *Q. J. R. Meteorol. Soc.* 146, 1999–2049. <https://doi.org/10.1002/qj.3803>

820 Hishinuma, S., Takeuchi, K., Magome, J., 2014. Challenges of hydrological analysis for water resource
821 development in semi-arid mountainous regions: case study in Iran. *Hydrol. Sci. J.* 59, 1718–1737.

822 Hong, Y., Hsu, K.-L., Sorooshian, S., Gao, X., 2004. Precipitation estimation from remotely sensed
823 imagery using an artificial neural network cloud classification system. *J. Appl. Meteorol.* 43, 1834–
824 1853.

825 Hosseini-Moghari, S.-M., Araghinejad, S., Ebrahimi, K., 2018. Spatio-temporal evaluation of global
826 gridded precipitation datasets across Iran. *Hydrol. Sci. J.* 63, 1669–1688.
827 <https://doi.org/10.1080/02626667.2018.1524986>

828 Hosseini-Moghari, S.-M., Tang, Q., 2020. Validation of GPM IMERG V05 and V06 Precipitation
829 Products over Iran. *J. Hydrometeorol.* 21, 1011–1037.

830 Hou, A.Y., Kakar, R.K., Neeck, S., Azarbarzin, A.A., Kummerow, C.D., Kojima, M., Oki, R., Nakamura,
831 K., Iguchi, T., 2014. The global precipitation measurement mission. *Bull. Am. Meteorol. Soc.* 95,
832 701–722.

833 Hsu, K., Gao, X., Sorooshian, S., Gupta, H. V, 1997. Precipitation estimation from remotely sensed
834 information using artificial neural networks. *J. Appl. Meteorol.* 36, 1176–1190.

835 Huffman, G.J., Adler, R.F., Arkin, P., Chang, A., Ferraro, R., Gruber, A., Janowiak, J., McNab, A.,
836 Rudolf, B., Schneider, U., 1997. The global precipitation climatology project (GPCP) combined
837 precipitation dataset. *Bull. Am. Meteorol. Soc.* 78, 5–20.

838 Huffman, G.J., Bolvin, D.T., Nelkin, E.J., Wolff, D.B., Adler, R.F., Gu, G., Hong, Y., Bowman, K.P.,
839 Stocker, E.F., 2007. The TRMM Multisatellite Precipitation Analysis (TMPA): Quasi-global,
840 multiyear, combined-sensor precipitation estimates at fine scales. *J. Hydrometeorol.* 8, 38–55.

841 Javanmard, S., Yatagai, A., Nodzu, M.I., BodaghJamali, J., Kawamoto, H., 2010. Comparing high-
842 resolution gridded precipitation data with satellite rainfall estimates of TRMM_3B42 over Iran.
843 *Adv. Geosci.* 25, 119–125.

844 Jiang, Q., Li, W., Fan, Z., He, X., Sun, W., Chen, S., Wen, J., Gao, J., Wang, J., 2021. Evaluation of the
845 ERA5 reanalysis precipitation dataset over Chinese Mainland. *J. Hydrol.* 595, 125660.

846 Joyce, R.J., Janowiak, J.E., Arkin, P.A., Xie, P., 2004. CMORPH: A method that produces global
847 precipitation estimates from passive microwave and infrared data at high spatial and temporal
848 resolution. *J. Hydrometeorol.* 5, 487–503.

849 Kalantari, Z., Ferreira, C.S.S., Koutsouris, A.J., Ahmer, A.K., Cerdà, A., Destouni, G., 2019. Assessing
850 flood probability for transportation infrastructure based on catchment characteristics, sediment
851 connectivity and remotely sensed soil moisture. *Sci. Total Environ.* 661, 393–406.
852 <https://doi.org/10.1016/j.scitotenv.2019.01.009>

853 Kalnay, E., Kanamitsu, M., Kistler, R., Collins, W., Deaven, D., Gandin, L., Iredell, M., Saha, S., White,
854 G., Woollen, J., 1996. The NCEP/NCAR 40-year reanalysis project. *Bull. Am. Meteorol. Soc.* 77,
855 437–472.

856 Katiraie-Boroujerdy, P.S., Akbari Asanjan, A., Hsu, K. lin, Sorooshian, S., 2017. Intercomparison of
857 PERSIANN-CDR and TRMM-3B42V7 precipitation estimates at monthly and daily time scales.
858 *Atmos. Res.* 193, 36–49. <https://doi.org/10.1016/j.atmosres.2017.04.005>

859 Katiraie-Boroujerdy, P.S., Nasrollahi, N., Hsu, K. lin, Sorooshian, S., 2013. Evaluation of satellite-based
860 precipitation estimation over Iran. *J. Arid Environ.* 97, 205–219.
861 <https://doi.org/10.1016/j.jaridenv.2013.05.013>

862 Katiraie Boroujerdy, P.S., 2013. Comparison of high-resolution gridded monthly satellite and ground-
863 based precipitation data over Iran. *Iran. J. Geophys.* 7, 149–160.

864 Khazaei, M.R., 2021. A robust method to develop future rainfall IDF curves under climate change
865 condition in two major basins of Iran. *Theor. Appl. Climatol.* 144, 179–190.

866 Kidd, C., Huffman, G., 2011. Global precipitation measurement. *Meteorol. Appl.* 18, 334–353.

867 Kling, H., Fuchs, M., Paulin, M., 2012. Runoff conditions in the upper Danube basin under an ensemble
868 of climate change scenarios. *J. Hydrol.* 424, 264–277.

869 Kobayashi, S., Ota, Y., Harada, Y., Ebata, A., Moriya, M., Onoda, H., Onogi, K., Kamahori, H.,
870 Kobayashi, C., Endo, H., 2015. The JRA-55 reanalysis: General specifications and basic

871 characteristics. *J. Meteorol. Soc. Japan. Ser. II* 93, 5–48.

872 Kucera, P.A., Ebert, E.E., Turk, F.J., Levizzani, V., Kirschbaum, D., Tapiador, F.J., Loew, A., Borsche,
873 M., 2013. Precipitation from space: Advancing Earth system science. *Bull. Am. Meteorol. Soc.* 94,
874 365–375.

875 Liu, Z., 2015. Comparison of precipitation estimates between Version 7 3-hourly TRMM Multi-Satellite
876 Precipitation Analysis (TMPA) near-real-time and research products. *Atmos. Res.* 153, 119–133.

877 Marjanizadeh, S., de Fraiture, C., Loiskandl, W., 2010. Food and water scenarios for the Karkheh River
878 Basin, Iran. *Water Int.* 35, 409–424.

879 Moazami, S., Golian, S., Hong, Y., Sheng, C., Kavianpour, M.R., 2016. Comprehensive evaluation of
880 four high-resolution satellite precipitation products under diverse climate conditions in Iran. *Hydrol.*
881 *Sci. J.* 61, 420–440.

882 Moazami, S., Golian, S., Kavianpour, M.R., Hong, Y., 2013. Comparison of PERSIANN and V7 TRMM
883 Multi-satellite Precipitation Analysis (TMPA) products with rain gauge data over Iran. *Int. J.*
884 *Remote Sens.* 34, 8156–8171.

885 Mosaffa, H., Shirvani, A., Khalili, D., Nguyen, P., Sorooshian, S., 2020. Post and near real-time satellite
886 precipitation products skill over Karkheh River Basin in Iran. *Int. J. Remote Sens.* 41, 6484–6502.
887 <https://doi.org/10.1080/01431161.2020.1739352>

888 Nashwan, M.S., Shahid, S., Dewan, A., Ismail, T., Alias, N., 2020. Performance of five high resolution
889 satellite-based precipitation products in arid region of Egypt: An evaluation. *Atmos. Res.* 236,
890 104809.

891 Novella, N.S., Thiaw, W.M., 2013. African rainfall climatology version 2 for famine early warning
892 systems. *J. Appl. Meteorol. Climatol.* 52, 588–606.

893 Onogi, K., Tsutsui, J., Koide, H., Sakamoto, M., Kobayashi, S., Hatsushika, H., Matsumoto, T.,
894 Yamazaki, N., Kamahori, H., Takahashi, K., 2007. The JRA-25 reanalysis. *J. Meteorol. Soc. Japan.*
895 *Ser. II* 85, 369–432.

896 Orsolini, Y., Wegmann, M., Dutra, E., Liu, B., Balsamo, G., Yang, K., Rosnay, P. de, Zhu, C., Wang, W.,
897 Senan, R., 2019. Evaluation of snow depth and snow cover over the Tibetan Plateau in global
898 reanalyses using in situ and satellite remote sensing observations. *Cryosph.* 13, 2221–2239.

899 Peyravi, M., Peyvandi, A.A., Khodadadi, A., Marzaleh, M.A., 2019. Flood in the South-West of Iran in
900 2019; causes, problems, actions and lesson learned. *Bull. Emerg. Trauma* 7, 199.

901 Qian, T., Dai, A., Trenberth, K.E., Oleson, K.W., 2006. Simulation of global land surface conditions from
902 1948 to 2004. Part I: Forcing data and evaluations. *J. Hydrometeorol.* 7, 953–975.

903 Raziei, T., Sotoudeh, F., 2017. Investigation of the accuracy of the European Center for Medium Range
904 Weather Forecast (ECMWF) in forecasting observed precipitation in different climates of Iran. *J.*
905 *earth Sp. Phys.* 43, 133–147.

906 Rienecker, M.M., Suarez, M.J., Gelaro, R., Todling, R., Bacmeister, J., Liu, E., Bosilovich, M.G.,
907 Schubert, S.D., Takacs, L., Kim, G.-K., 2011. MERRA: NASA's modern-era retrospective analysis
908 for research and applications. *J. Clim.* 24, 3624–3648.

909 Roebber, P.J., 2009. Visualizing multiple measures of forecast quality. *Weather Forecast.* 24, 601–608.

910 Sabater, M., Data, J.E.-L.M.A., 2019. from 1981 to Present. Copernicus Clim. Chang. Serv. Clim. Data
911 Store.

912 Salio, P., Hobouchian, M.P., Skabar, Y.G., Vila, D., 2015. Evaluation of high-resolution satellite
913 precipitation estimates over southern South America using a dense rain gauge network. *Atmos. Res.*
914 163, 146–161.

915 Satgé, F., Defrance, D., Sultan, B., Bonnet, M.P., Seyler, F., Rouché, N., Pierron, F., Paturel, J.E., 2020.
916 Evaluation of 23 gridded precipitation datasets across West Africa. *J. Hydrol.* 581, 124412.
917 <https://doi.org/10.1016/j.jhydrol.2019.124412>

918 Schneider, U., Becker, A., Finger, P., Meyer-Christoffer, A., Rudolf, B., Ziese, M., 2011. GPCP full data
919 reanalysis version 6.0 at 0.5: Monthly land-surface precipitation from rain-gauges built on GTS-
920 based and historic data. *GPCC Data Rep.*, doi 10.

921 Schneider, U., Fuchs, T., Meyer-Christoffer, A., Rudolf, B., 2008. Global precipitation analysis products
922 of the GPCC. *Glob. Precip. Climatol. Cent. (GPCC), DWD, Internet Publ.* 112.

923 Schulzweida, U., 2019. CDO user guide. *Clim Data Oper.*

924 Sharifi, E., Steinacker, R., Saghafian, B., 2016. Assessment of GPM-IMERG and other precipitation
925 products against gauge data under different topographic and climatic conditions in Iran: Preliminary
926 results. *Remote Sens.* 8, 135.

927 Shayeghi, A., Azizian, A., Brocca, L., 2020. Reliability of reanalysis and remotely sensed precipitation
928 products for hydrological simulation over the Sefidrood River Basin, Iran. *Hydrol. Sci. J.* 65, 296–
929 310. <https://doi.org/10.1080/02626667.2019.1691217>

930 Sheffield, J., Goteti, G., Wood, E.F., 2006. Development of a 50-year high-resolution global dataset of
931 meteorological forcings for land surface modeling. *J. Clim.* 19, 3088–3111.

932 Shen, Z., Yong, B., Gourley, J.J., Qi, W., Lu, D., Liu, J., Ren, L., Hong, Y., Zhang, J., 2020. Recent
933 global performance of the Climate Hazards group Infrared Precipitation (CHIRP) with Stations
934 (CHIRPS). *J. Hydrol.* 591, 125284.

935 Sorooshian, S., Hsu, K.L., Gao, X., Gupta, H. V., Imam, B., Braithwaite, D., 2000. Evaluation of
936 PERSIANN system satellite-based estimates of tropical rainfall. *Bull. Am. Meteorol. Soc.* 81, 2035–
937 2046. [https://doi.org/10.1175/1520-0477\(2000\)081<2035:EOPSSE>2.3.CO;2](https://doi.org/10.1175/1520-0477(2000)081<2035:EOPSSE>2.3.CO;2)

938 Sun, Q., Miao, C., Duan, Q., Ashouri, H., Sorooshian, S., Hsu, K., 2018. A Review of Global
939 Precipitation Data Sets: Data Sources, Estimation, and Intercomparisons. *Rev. Geophys.* 56, 79–
940 107. <https://doi.org/10.1002/2017RG000574>

941 Tong, K., Su, F., Yang, D., Hao, Z., 2014. Evaluation of satellite precipitation retrievals and their
942 potential utilities in hydrologic modeling over the Tibetan Plateau. *J. Hydrol.* 519, 423–437.

943 Ushio, T., Sasashige, K., Kubota, T., Shige, S., Okamoto, K., Aonashi, K., Inoue, T., Takahashi, N.,
944 Iguchi, T., Kachi, M., 2009. A Kalman filter approach to the Global Satellite Mapping of
945 Precipitation (GSMaP) from combined passive microwave and infrared radiometric data. *J.*
946 *Meteorol. Soc. Japan. Ser. II* 87, 137–151.

947 Vaghefi, S.A., Keykhai, M., Jahanbakhshi, F., Sheikholeslami, J., Ahmadi, A., Yang, H., Abbaspour,
948 K.C., 2019. The future of extreme climate in Iran. *Sci. Rep.* 9, 1–11.

949 Wilks, D.S., 2011. Statistical methods in the atmospheric sciences. Academic press.

950 Yatagai, A., Kamiguchi, K., Arakawa, O., Hamada, A., Yasutomi, N., Kitoh, A., 2012. APHRODITE:
951 Constructing a long-term daily gridded precipitation dataset for Asia based on a dense network of
952 rain gauges. *Bull. Am. Meteorol. Soc.* 93, 1401–1415.

953 Yong, B., Liu, D., Gourley, J.J., Tian, Y., Huffman, G.J., Ren, L., Hong, Y., 2015. Global view of real-
 954 time TRMM multisatellite precipitation analysis: Implications for its successor global precipitation
 955 measurement mission. *Bull. Am. Meteorol. Soc.* 96, 283–296.

956 Yuan, F., Zhang, L., Win, K.W.W., Ren, L., Zhao, C., Zhu, Y., Jiang, S., Liu, Y., 2017. Assessment of
 957 GPM and TRMM multi-satellite precipitation products in streamflow simulations in a data-sparse
 958 mountainous watershed in Myanmar. *Remote Sens.* 9, 302.

959 Zambrano-Bigiarini, M., 2014. hydroGOF: Goodness-of-fit functions for comparison of simulated and
 960 observed hydrological time series. R Packag. version 0.3-8.

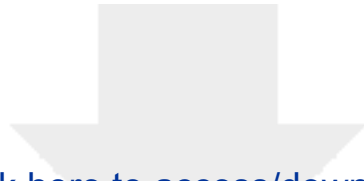
961 Zhang, Q., Sun, P., Singh, V.P., Chen, X., 2012. Spatial-temporal precipitation changes (1956–2000) and
 962 their implications for agriculture in China. *Glob. Planet. Change* 82, 86–95.

963 Zhang, X., Kang, T., Wang, H., Sun, Y., 2010. Analysis on spatial structure of landuse change based on
 964 remote sensing and geographical information system. *Int. J. Appl. Earth Obs. Geoinf.* 12.
 965 <https://doi.org/10.1016/j.jag.2010.04.011>

966

- 1 **Conflict of interests:** The authors declare no conflict of interest





[Click here to access/download](#)

Interactive Map Data (.kml, .kmz)
Karkhe and Karun Basin.kml

